Joint Power Allocation and Beam Scheduling in Beam-Hopping Satellites: A Two-Stage Framework with a Probabilistic Perspective

Lin Chen, *Graduate Member, IEEE*, Linlong Wu, *Senior Member, IEEE*, Eva Lagunas, *Senior Member, IEEE*, Anyue Wang, Lei Lei, *Senior Member, IEEE*, Symeon Chatzinotas, *Fellow, IEEE*, Björn Ottersten, *Fellow, IEEE*

***Abstract*—Beam-hopping (BH) technology, integral to multi-beam satellite systems, adapts beam activation to the variable communication demands of terrestrial users. The optimization of power allocation and beam illumination scheduling constitutes the core design challenge in BH systems, especially under the constraint on a limited number of simultaneously active beams due to restricted radio frequency chain availability. This paper proposes a two-stage BH design solution, which minimizes energy consumption in BH satellite communications while accommodating the heterogeneous demands of users. The first stage addresses the coupling variables of power and beam status by recasting the allocation and scheduling problem through a statistical lens, thus breaking down the intricate relationship between variables. To manage the resulting non-convex challenge, we propose an iterative method that capitalizes on the optimality conditions inherent to this problem. This method is designed to procure a statistically-informed solution that aligns with our reformulated interpretation. Subsequently, the second stage maps this solution into a concrete beam illumination schedule, employing binary quadratic programming techniques. A penalty-based iterative method is applied, ensuring convergence to a locally optimal solution. Through numerical simulations, the proposed framework has been validated for its efficacy in improving energy efficiency and accurately matching demands.**

***Index Terms*—Energy minimization, power control, beam hopping, binary quadratic programming**

I. Introduction

Satellite communications (SatCom) are widely acknowledged for their capability to offer pervasive connectivity and reliable data transfer, utilizing high-altitude satellites to encompass extensive geographic regions. Historically used for television broadcasting through single-beam Geostationary (GEO) satellites, the technology has advanced significantly since the 2000s. The evolution has led to multi-beam high-throughput satellites that operate in the higher frequency ranges (i.e., Ku and Ka bands) and cater to the broadband market [1]. Nowadays, SatCom's capabilities to connect anyone, anywhere, and anytime are considered a key feature to extend terrestrial 5G cellular connectivity to unreachable areas [2].

Current broadband satellite communication systems typically use a static beam configuration where the coverage is evenly divided into hundreds of spot-beam areas. To avoid interfering among beams, the operator schedules the active beams using an orthogonal frequency reuse strategy. However, this method is frequency-inefficient, which has motivated the development of more adaptable payload designs [3, 4].

To address this challenge, the concept of Beam-Hopping (BH)-enabled satellite communication systems has been introduced [5]. Unlike traditional fixed-beam systems, BH systems only activate a subset of spot beams within a designated period, known as "dwell time." These active beams can be changed dynamically, following a beam illumination plan that responds to varying demands.

Beam-hopping offers numerous benefits, the most significant being the temporal flexibility it provides in distributing capacity to different beams as needed. Additionally, activating fewer beams at any given time requires fewer onboard Radio Frequency (RF) chains, which can reduce spacecraft weight and size. Ultimately, this reduction may result in decreased launch costs.

BH satellite communication technology has reached a level of maturity, significantly bolstered by industry support. This support has led to adaptations, such as the standardization of satellite air interfaces, to accommodate BH synchronization needs [6, 7]. An example of this technology in action is the Eutelsat Quantum satellite, which employs forward link BH. While the technical capability for beam illumination and configuration exists, the effective management of these functions remains an active area of research and development. This is mainly because crafting an optimal beam time-activation plan and allocating power effectively is complex. Specifically, it is challenging to properly allocate the limited satellite power across all active beams to meet the dynamic demands while satisfying the satellite payload hardware limitations.

SatCom systems should carefully manage energy consump-

This work was supported by the Luxembourg National Research Fund (FNR) under the project "FlexSAT: Resource Optimization for Next Generation of Flexible SATellite Payloads" (C19/IS/13696663). Lin Chen, Linlong Wu, Eva Lagunas, Anyue Wang, Symeon Chatzinotas, and Björn Ottersten are with the Interdisciplinary Centre for Security, Reliability and Trust (SnT), University of Luxembourg, Luxembourg. The work of L. Wu was supported by the Luxembourg National Research Fund (FNR) through the CORE INTER project under C20/IS/14799710/SENCOM. Lei Lei is with the School of Information and Communications Engineering, Xi'an Jiaotong University, Xi'an, China. The work of L. Lei was supported in part by the National Key Laboratory Foundation under Grant HTKJ2023KL504002 and 2023-JCJQ-LB-007; in part by the Qin Chuangyuan Innovation and Talent Project under Grant QCYRCXM-2023-049; in part by the Key Research and Development Program of Shaanxi under Grant 2024GX-YBXM-065. *(Corresponding author: Lin Chen)*

tion. Satellite payloads are equipped with solar panels that convert solar energy into electricity, which powers wireless transmission and other operations [8]. Given that these panels can only collect a limited amount of power, it is crucial for these systems to address the issue of energy efficiency. Additionally, excessive energy consumption can have adverse effects on the payload's mass and lifespan [9]. As a consequence, the minimization of transmit power has become a significant area of research for general non-terrestrial communication platforms, e.g. [10].

In recent years, flexible resource allocation strategies for satellite communication systems have attracted considerable attention. For instance, [11] offers a design and analysis of the beam illumination pattern for BH systems, aiming to optimally match the traffic demands. In [12], [13], and [14] BH is combined with interference mitigation techniques to enable the simultaneous activation of adjacent beams, using the same spectral resources. Notably, [14] proposed to design the illumination pattern by penalizing the activation of adjacent beams, with the aim of reducing the usage of precoding techniques whenever possible. Other works, like [15], and [16], proposed to design the illumination pattern via deep learning techniques. These works focus only on exploring the flexibility in the time domain, which does not fully utilize the capabilities of onboard resources. Power allocation for non-BH satellite systems has also been evaluated. In [17], the authors propose allocating power based on traffic demands and channel conditions. An energy-aware power allocation problem for non-BH systems is formulated in the work [9], which aims to minimize both unmet system capacity and total radiated power. Both [17] and [9] consider only the flexibility of onboard resources in the power domain. Although [18] proposed jointly allocating power and frequency carriers to minimize the weighted objective of energy consumption and frequency occupation, the proposed design does not fully utilize the precious spectrum resources. The load coupling model, originally analyzed by [19], characterizes the coupling relationships among the temporal occupation of beams. The model has been employed, for instance, in [20], the work most closely related to ours, where the power and load of beams are studied for cellular networks to minimize the energy consumption. However, [20] does not consider the constraint on the maximal number of simultaneously active beams, an issue that is addressed in our work.

Based on the existing works, we consider the joint design of beam illumination patterns and power allocation to optimize the energy efficiency of the BH satellite system, which has a limit on the maximum number of simultaneously active beams. Intrinsically, the beam pattern and the corresponding power assignment are coupled, both of which contribute to the achievable capacity and therefore influence the overall energy consumption. To the best of our knowledge, this challenge has not been effectively addressed in the literature to date.

To address the challenge stated above, we propose a two-stage framework to solve the combinatorial nonconvex problem. In the first stage, utilizing the mean-field theory [21, 22], we reinterpret the beam illumination patterns with beam activation probabilities, consequent to which the corresponding power will be the average one for the whole time window. Accordingly, the original problem is reformulated into a new one, where the average powers and activation probabilities of the beams are the optimization variables. An iterative method is also proposed to solve this problem optimally. In the second stage, the activation probabilities of the solution obtained in the first stage are mapped into the discrete beam illumination patterns by solving a binary quadratic programming problem.

Our major contributions are summarized as follows:

- We propose a two-stage framework to jointly design power allocation and beam scheduling for BH satellite systems. Within the framework, by utilizing the mean-field theory, a probabilistic reformulation becomes available which paves the way for addressing the intrinsic coupling between beam power and beam illumination pattern. Besides, for the reformulated problem, we analyze the optimality conditions and develop an iterative method to yield a globally optimal solution.
- We also develop a systematic mapping scheme that converts the probabilistic solution obtained in the first stage into a deterministic one satisfying all constraints. To ensure the practicality of the solution, beam hopping latency is also integrated into the scheme.
- Numerical simulation results validate the theoretical findings: i) the system consumes minimal energy when all available beams are active during the time window; ii) increasing the maximal number of active beams could reduce energy consumption. Furthermore, given that our mathematical model is based on the Shannon formula, we acknowledge a potential performance loss due to coding modulation methods in real-world applications. To address this concern, our study includes a method specifically designed to compensate for such performance loss, ensuring the completeness and applicability of our approach in practical scenarios.

The remainder of the paper is organized as follows. In section II, we present the system model and formulate the energy minimization problem from a deterministic perspective. In section III, we reformulate the problem from a statistical perspective. Section IV, we focus on solving the statistical problem, and we simply introduce the method to convert the statistical solution to design the deterministic illumination pattern in Section V. In Section VI, we validate the proposed framework with numerical simulations. The conclusion is made in Section VII.

II. System Model and Problem Formulation

In this section, we first introduce the system model for the considered beam-hopping satellite system and then formulate the problem of energy efficiency, which minimizes the total consumed energy while satisfying both the limited onboard resources and on-ground user demands.

A. System Model for Beam-Hopping Satellite

A bent-pipe multi-beam geostationary orbit (GEO) satellite system is considered for the forward-link transmission. The system covers the area of service by N spot beams, each of

TABLE I: Glossary of notations

Notation	Definition
B	Available full bandwidth
K	Maximal number of simultaneously active beams
M	Total number of TSs within the time window
N	Total number of beams
$\mathbf{d}$	Vector of demands in bps
$\hat{\mathbf{d}}$	Vector of demands in [number of TSs]
$\mathbf{H}$	The channel matrix
$p_{n,t}$	Transmit power of beam n at TS t
p_n	Average transmit power of beam n
$\mathbf{p}$	Vector of the average transmit power
$\mathbf{P}$	Penalty matrix
$x_{n,t}$	Beam activation indicator n at TS t
$\mathbf{y}$	Vector of consumed energy of beams
$\boldsymbol{\rho}$	Vector of activation probability of beams
ΔT	Duration of TS
$\sigma(\cdot)$	Spectral radius of the matrix
σ_T^2	Power of thermal noise
$g(\rho_n)$	$\rho_n(2^{\frac{d_n}{B\rho_n}}-1)$
$\mathbf{G}_i$	$\mathtt{Diag}(\mathbf{g}(\boldsymbol{\rho}_i)),\quad i=0,1,2$
τ	Latency trade-off factor
ϵ	Demand compensation coefficient
$\mathtt{dim}(\cdot)$	The dimension of the vector
$\lfloor\cdot\rfloor$	The minimal integer of the value

which reuses the same spectrum of the bandwidth B. The BH time window for the system is composed of M consecutive time slots (TSs) with time-slot duration $\triangle T$. The considered system configurations are compliant with the satellite DVB-S2(X) standard [23] air interface, where the superframes duration [24] corresponds to the minimum switching time $\triangle T$ defined above. For such a system, we aim to design the beam illumination pattern, which assigns these N beams over the M time slots within the time window.

Let $\mathbf{H} \in \mathbb{C}^{N\times N}$ be the channel matrix containing all the channel coefficients of the forward link. In particular, the channel coefficient corresponding to the n-th satellite beam to the user k is modeled following the approach in [25], and can be written as,

$$H_{n,k} = \sqrt{G_k^{Rx} G_n^{Tx}(x_k, y_k)} e^{j\phi_{n,k}} / (4\pi \frac{D_k}{\lambda}) \tag{1}$$

where G_k^{Rx} denotes the receive antenna gain of the user k; $G_n^{Tx}(x_k, y_k)$ denotes the transmit antenna gain from the n-th satellite beam to the user k, which is located at the longitude x_k and latitude y_k; $\phi_{n,k}$ is the phase component associated with the n-th satellite beam and the user k; λ denotes the wavelength of the carrier frequency band; D_k denotes the distance between the satellite and the user k.

Note that our main focus is on beam-demand satisfaction, concentrating on beam scheduling rather than ground user scheduling, which is beyond the scope of this work. Accordingly, a super-user terminal is modeled, which essentially aggregates all user's demands and is served by one of the N beams. This abstraction is compliant with the unicast transmission mode typically employed in the DVB-S2(X) air interface, where the multiplexing of users is done via Time-Division Multiple Access (TDMA). Thus given this one-to-one mapping between beam and super-user, the index n interchangeably refers to both the satellite beam and super-user terminal.

We denote the traffic demand for beam n as d_n with unit bps, and the vector of demands of all beams as $\mathbf{d} = [d_1, \ldots, d_N]^T$. We denote the transmit power for beam n at TS t by $p_{n,t}, \forall n = 1, \ldots, N, t = 1 \ldots, M$. The activation of beam n at TS t is indicated by $x_{n,t} \in \{0, 1\}$ with $x_{n,t} = 1$ if the beam is activated and $x_{n,t} = 0$ otherwise.

The achievable rate of the terminal in beam n at TS t is

$$R_n[t] = B\log_2(1 + \frac{p_{n,t}|H_{n,n}|^2}{\sum_{i\neq n} p_{i,t}|H_{i,n}|^2 + \sigma_T^2}), \tag{2}$$

where $\sigma_T^2 = \tau T_{Rx} B$ represents the thermal noise power with τ being the Boltzmann constant, and T_{Rx} being the clear sky noise temperature of the receiver [25].

Therefore, the demand constraint is

$$\frac{1}{M}\sum_{t=1}^{M} R_n[t] \geq d_n,\ \forall n, \tag{3}$$

which ensures that the average achievable rate within the M TSs is no less than the requested traffic demand of the n-th beam.

B. Problem Formulation of Energy Minimization

We formulate a resource allocation problem to jointly optimize power allocation and beam illumination to minimize the total consumed energy while satisfying uneven beam demands. Therefore, the problem, denoted as $\mathcal{P}_0$, is formulated as

$$\mathcal{P}_0 \begin{cases} \underset{p_{n,t}}{\mathtt{minimize}} & \sum_{t=1}^{M}\sum_{n=1}^{N} p_{n,t} \\ \mathtt{subject\ to} & (C_1): \frac{1}{M}\sum_{t=1}^{M} R_n[t] \geq d_n,\ \forall n, \\ & (C_2): \sum_{n=1}^{N} x_{n,t} \leq K,\ \forall t, \\ & (C_3): p_{n,t} \geq 0,\ \forall n, t, \\ & (C_4): x_{n,t} = \mathtt{sign}(p_{n,t}),\ \forall n, t, \end{cases}$$

where $R_n[t]$ is defined by Eq. (2), and $\mathtt{sign}(\cdot)$ is the sign function. The problem is subject to four constraints: C_1, the demand constraint, C_2, the maximum number of simultaneously active beams, C_3, the non-negativity of $p_{n,t}$, and C_4, the binarization of $x_{n,t}$. Among these constraints, C_2 is incroporated. Due to the mass limit of the satellite payload, the maximum number of simultaneously active beams should not exceed the number of digital RF chains, denoted as $K(K \leq N)$. The constraint is a key feature of BH-based SatCom systems, as it enables a significant reduction in satellite mass. $\mathcal{P}_0$ is a non-convex mixed-integer programming problem, which poses significant challenges in finding a solution.

III. Problem Reformulation via Mean Field Theory

For a conventional approach to mixed integer programming problems, it first relaxes the binary variable $x_{n,t}$ to be continuous and linearizes the demand constraint with respect to

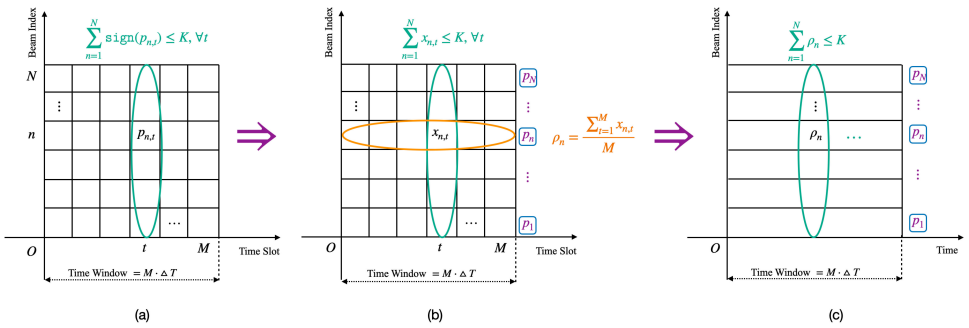

Fig. 1: The formulation and reformulation of the problem. (a) the original problem $\mathcal{P}_0$; (b) the intermediate status of the problem conversion; (c) the reformulated problem $\mathcal{P}_1$.

$p_{n,t}$. Subsequently, the variables are alternatively updated with iterations.

However, the variables of $\mathcal{P}_0$ are coupled, making this typical approach less suitable. Furthermore, popular learning methods such as deep learning often require a large dataset for model training. Given the aforementioned challenges, properly addressing the strong coupling relationship between $p_{n,t}$ and $x_{n,t}$ is crucial for efficiently solving the problem $\mathcal{P}_0$. To achieve this, we employ the Mean Field Theory (MFT) [21, 22] to decouple the power and beam activation indicators.

In the mean-field method, the mutual influence between random variables is replaced by an effective field, which acts independently on each random variable [21]. Considering that the power variable $p_{n,t}$ serves dual functions — representing both the power value and potentially indicating the status of the beam at a given instance of TS— these variables are mutually influenced in the time domain via the demand constraint C_1. To simplify the problem, we apply the Mean Field Theory method, which replaces the power vector variable with its average power across all beams. This is followed by replacing the indicator vector variable with its activation probability. We summarize the reformulation progress graphically in Fig. 1.

Specifically, suppose that we have obtained the optimal solution to $\mathcal{P}_0$, denoted by $(p_{n,t}, x_{n,t}), \forall n, t$. We define p_n and ρ_n as the average power and activation probability, respectively, over the entire time window for beam n across all beams. The variable ρ_n represents the probability that beam n is activated during the time window of the optimal solution, and is defined as $\rho_n = \frac{\sum_{t=1}^{M} x_{n,t}}{M} \in (0, 1]$.

Accordingly, the total energy consumption can be reformulated as the total expected consumed energy, $\boldsymbol{\rho}^T \mathbf{p} \cdot \triangle T$, where $\boldsymbol{\rho} = [\rho_1, \ldots, \rho_N]^T$ and $\mathbf{p} = [p_1, \ldots, p_N]^T$. The number of simultaneously active beams can be expressed as the expected number of active beams, $\boldsymbol{\rho}^T \mathbf{1}$. Regarding the demand constraint C_1, it can be reformulated to ensure the expected capacity meets its demand as follows.

$$\rho_n B \log_2(1 + \frac{p_n |H_{n,n}|^2}{\sum_{i \neq n} \rho_i p_i |H_{i,n}|^2 + \sigma_T^2}) \geq d_n, \ \forall n. \quad (5)$$

which can be further rewritten as

$$\rho_n \geq f_n(\boldsymbol{\rho}, \mathbf{p}) \triangleq \frac{d_n}{B \log_2(1 + \frac{p_n |H_{n,n}|^2}{\sum_{i \neq n} \rho_i p_i |H_{i,n}|^2 + \sigma_T^2})}, \ \forall n. \quad (6)$$

Therefore, $\mathcal{P}_0$ can be reformulated as

$$\mathcal{P}_1 \begin{cases} \underset{\boldsymbol{\rho}, \mathbf{p}}{\texttt{minimize}} & \boldsymbol{\rho}^T \mathbf{p} \\ \texttt{subject to} & (\hat{C}_1) : \boldsymbol{\rho} \succeq \mathbf{f}(\boldsymbol{\rho}, \mathbf{p}), \\ & (\hat{C}_2) : \boldsymbol{\rho}^T \mathbf{1} \leq K, \\ & (\hat{C}_3) : \mathbf{p} \succ \mathbf{0}, \\ & (\hat{C}_4) : \mathbf{0} \prec \boldsymbol{\rho} \preceq \mathbf{1}, \end{cases}$$

where $\mathbf{f}(\boldsymbol{\rho}, \mathbf{p}) = [f_1(\boldsymbol{\rho}, \mathbf{p}), \ldots, f_N(\boldsymbol{\rho}, \mathbf{p})]^T$. The curled inequality symbol $\succeq$ (and its strict form $\succ$) is used to denote a generalized component-wise inequality between vectors. The vectors $\mathbf{0}$ and $\mathbf{1}$ are the ones with all elements being 0 and 1, respectively.

Note that the solution of $\mathcal{P}_1$ is in terms of activation probabilities of the N beams, which need to be converted into a discrete illumination pattern. This conversion method will be developed in Section V. In the next section, we will focus on solving $\mathcal{P}_1$.

IV. First-stage: Probabilistic Beam Hopping Solution

In this section, our focus is on solving the non-convex problem $\mathcal{P}_1$. The conventional approach might involve linearizing constraint $\hat{C}_1$ first and then updating the two variables through iterations [18]. However, this approach often leads to performance loss due to the approximation error between the original and linearized versions and is typically time-consuming. In this work, we propose a novel method that optimally solves the problem. Briefly, we first prove that the fixed point satisfying $\boldsymbol{\rho} = \mathbf{f}(\boldsymbol{\rho}, \mathbf{p})$ is a necessary condition for the optimum of $\mathcal{P}_1$. Based on this necessary condition, the optimal power can be expressed as a function of the optimal activation probability. Consequently, the objective of the problem boils down to an inverse matrix optimization problem, which we have further demonstrated is equivalent to a convex problem.

A. Necessary Condition for the Feasible Problem $\mathcal{P}_1$

According to [26], a fixed point of a function is a point that the function maps to itself, i.e. $x = 1$ is a fixed point of the function $f(x) = x^2$ because $f(1) = 1$. In nonlinear programming, the characteristics of the fixed point can be

utilized to devise iterative methods for finding solutions [27]. The following theorem indicates that the solution to $\mathcal{P}_1$ is a fixed point.

***Theorem** 1:* Given $\mathbf{d}, \mathbf{H}$, and K, the solution to the problem $\mathcal{P}_1$, if it exists, is the fixed point of the equations: $\boldsymbol{\rho} = \mathbf{f}(\boldsymbol{\rho}, \mathbf{p})$.

Proof: The proof is in Appendix A. ∎

Theorem 1 illustrates the coupling relationship between power and activation probability. Intuitively, a change in demand for one beam can strongly affect the solutions of adjacent beams and, consequently, the entire system. This observation validates the theorem and leads to the following corollary.

Corollary 1: Denoting the relationship between the optimal activation probability $\boldsymbol{\rho}$ and the optimal power $\mathbf{p}$ as $\mathbf{p} = \hat{\mathbf{f}}(\boldsymbol{\rho})$, the function $\hat{\mathbf{f}}(\cdot)$ is a one-to-one mapping.

Proof: Theorem 1 states that the fixed point is the necessary condition of the solution to the $\mathcal{P}_1$. Given the fixed point equation $\rho_n = f_n(\boldsymbol{\rho}, \mathbf{p}), \forall n$, we can derive the followings.

$$d_n = \rho_n B \log_2(1 + \frac{p_n |H_{n,n}|^2}{\sum_{i \neq n} \rho_i p_i |H_{i,n}|^2 + \sigma_T^2}) \tag{8a}$$

$$\Rightarrow \quad p_n = (2^{\frac{d_n}{B\rho_n}} - 1)(\sum_{i \neq n} \rho_i p_i \frac{|H_{i,n}|^2}{|H_{n,n}|^2} + \frac{\sigma_T^2}{|H_{n,n}|^2}) \tag{8b}$$

$$\Rightarrow \rho_n p_n = \rho_n (2^{\frac{d_n}{B\rho_n}} - 1)(\sum_{i \neq n} \rho_i p_i \frac{|H_{i,n}|^2}{|H_{n,n}|^2} + \frac{\sigma_T^2}{|H_{n,n}|^2}) \tag{8c}$$

$$\Rightarrow \quad y_n = g(\rho_n)(\sum_{i \neq n} y_i A_{i,n} + b_n) \tag{8d}$$

where we denote matrix $\mathbf{A}$ with elements $A_{n,n} = 0$, and $\forall i \neq n, A_{i,n} = \frac{|H_{i,n}|^2}{|H_{n,n}|^2}$; $b_n = \frac{\sigma_T^2}{|H_{n,n}|^2}$; $g(\rho_n) = \rho_n(2^{\frac{d_n}{B\rho_n}} - 1)$; and $y_n = \rho_n p_n$, representing the consumed energy of the n-th beam.

According to (8d), we denote the vector of all beams' consumed energies by $\mathbf{y} = [y_1, \ldots, y_N]^T$ and establish its relationship with the vector $\boldsymbol{\rho}$ compactly as follows:

$$\mathbf{y} = (\mathbf{I} - \mathbf{GA})^{-1}\mathbf{Gb} \tag{9a}$$

$$\Rightarrow \mathbf{p} = \mathtt{Diag}(\boldsymbol{\rho}^{-1})(\mathbf{I} - \mathbf{GA})^{-1}\mathbf{Gb} \tag{9b}$$

where $\mathbf{G} = \mathtt{Diag}(\mathbf{g}(\boldsymbol{\rho}))$, and $\mathbf{g}(\boldsymbol{\rho}) = [g(\rho_1), \ldots, g(\rho_N)]^T$. $\mathtt{Diag}(\mathbf{x})$ denotes the diagonal matrix with diagonal elements given by vector $\mathbf{x}$, and $\mathbf{I}$ is the identity matrix. Finally, $\mathbf{b} = [b_1, \ldots, b_N]^T$.

Eq. (9b) indicates that the relationship between the optimal power and the activation probability is a one-to-one mapping and thereby completes the proof. ∎

Based on Eq. (9a), $\mathcal{P}_1$ is equivalent to

$$\mathcal{P}_2 \begin{cases} \underset{\boldsymbol{\rho}}{\mathtt{minimize}} & \mathbf{1}^T(\mathbf{I} - \mathbf{G}(\boldsymbol{\rho})\mathbf{A})^{-1}\mathbf{G}(\boldsymbol{\rho})\mathbf{b} \\ \mathtt{subject\ to} & (\hat{C}_2): \boldsymbol{\rho}^T\mathbf{1} \leq K \\ & (\tilde{C}_3): \sigma(\mathbf{G}(\boldsymbol{\rho})\mathbf{A}) < 1 \\ & (\hat{C}_4): \mathbf{0} \prec \boldsymbol{\rho} \preceq \mathbf{1} \end{cases}$$

where $\mathbf{G}(\boldsymbol{\rho}) = \mathtt{Diag}(\mathbf{g}(\boldsymbol{\rho}))$ is a function of $\boldsymbol{\rho}$ and will be denoted as $\mathbf{G}$ for simplicity. $\sigma(\mathbf{X})$ denotes the spectral radius of the matrix $\mathbf{X}$ – the largest absolute eigenvalue of $\mathbf{X}$.

The constraint $\tilde{C}_3$ in $\mathcal{P}_2$ corresponds to the constraint $\hat{C}_3$ in $\mathcal{P}_1$. Note that $\forall \boldsymbol{\rho} \succ \mathbf{0}$, there holds $\mathbf{G} \succ \mathbf{0}$. Additionally, $\mathbf{b} \succ \mathbf{0}, \mathbf{A} \succ \mathbf{0}$ for all times. According to Eq. (9b), given $\boldsymbol{\rho} \succ \mathbf{0}$, the positivity of $\mathbf{p}$ is equivalent to the positivity of the matrix $(\mathbf{I} - \mathbf{GA})^{-1}$ which is determined by the spectral radius of the matrix $\mathbf{GA}$. The following Theorem 2 provides a detailed explanation.

***Theorem** 2:* Given $\mathbf{d}, \mathbf{H}$ and K, a feasible positive solution of the Eq. (9b) exists if and only if there exists a $\boldsymbol{\rho}$ such that the spectral radius of the matrix $\mathbf{GA}$ is less than 1, i.e. $\sigma(\mathbf{GA}) < 1$.

Proof: The proof is given by the [28, Theorem 1]. ∎

Theorem 2 establishes the necessary condition for the feasibility of the solution to $\mathcal{P}_2$.

B. Convexity Analysis of Problem $\mathcal{P}_2$

$\mathcal{P}_2$ involves matrix inverse and spectral radius, making it challenging to solve in general. However, by analyzing and exploiting the special structures of the constraints and the objective function, we demonstrate that solving $\mathcal{P}_2$ is equivalent to solving a convex problem. This insight paves the way for obtaining the global optimal solution to $\mathcal{P}_1$.

Lemma 1: Given B, d, the function $g(z) = z(2^{\frac{d}{Bz}} - 1)$ is monotonically decreasing and convex in the domain $z \in (0, +\infty)$

Proof: The proof is in Appendix B. ∎

Lemma 2: Given $\mathbf{H}, \mathbf{d}$, the set $\mathcal{Y} = \{\boldsymbol{\rho} | \sigma(\mathbf{GA}) \leq 1, \mathbf{0} \preceq \boldsymbol{\rho} \preceq \mathbf{1}\}$ is convex.

Proof: The proof is in Appendix C. ∎

In the proof presented in Appendix C, we define the condition to determine whether the given parameters $\mathbf{H}, \mathbf{d}$ are reasonable. When given reasonable parameters, the set $\mathcal{Y}$ is non-empty.

***Theorem** 3:* The solution to $\mathcal{P}_2$ is equivalent to the solution to a convex problem, which is given by

$$\mathcal{P}_3 : \underset{\boldsymbol{\rho} \in \hat{\mathcal{Y}}}{\mathtt{minimize}} \quad L(\boldsymbol{\rho}) \tag{11}$$

where $\hat{\mathcal{Y}} = \mathcal{Y} \cap \{\boldsymbol{\rho} | \boldsymbol{\rho}^T\mathbf{1} \leq K\}$, and

$$L(\boldsymbol{\rho}) = \begin{cases} \mathbf{1}^T(\mathbf{I} - \mathbf{GA})^{-1}\mathbf{Gb} & \boldsymbol{\rho} \in \hat{\mathcal{Y}} \setminus \{\boldsymbol{\rho} | \sigma(\mathbf{GA}) = 1\} \\ +\infty & \boldsymbol{\rho} \in \{\boldsymbol{\rho} | \sigma(\mathbf{GA}) = 1\} \end{cases} \tag{12}$$

Proof: The proof is in Appendix D. ∎

Previously, we explored the problem theoretically. Next, we will graphically illustrate the potential characteristics of the optimum, providing the basis for mapping the statistical solution to the deterministic one in Section V.

Lemma 3: Given reasonable $\mathbf{d}, \mathbf{H}$, i.e. $\mathcal{Y} \neq \emptyset$, the feasibility of $\mathcal{P}_3$ depends on the parameter K, which represents the maximum number of active beams. If K is small, the problem may be infeasible. However, increasing K may render an initially infeasible problem feasible.

Proof: The feasible set of $\mathcal{P}_3$ is the intersection of two convex sets, i.e., $\hat{\mathcal{Y}} = \mathcal{Y} \cap \{\boldsymbol{\rho} | \boldsymbol{\rho}^T\mathbf{1} \leq K\}$, thus it is convex.

According to *Lemma* 2, given reasonable $\mathbf{H}, \mathbf{d}$, the set $\mathcal{Y}$ is convex and non-empty. Therefore, whether the set $\hat{\mathcal{Y}}$ is empty is determined by the parameter K. Additionally, for $\forall \boldsymbol{\rho}_1 \succeq$

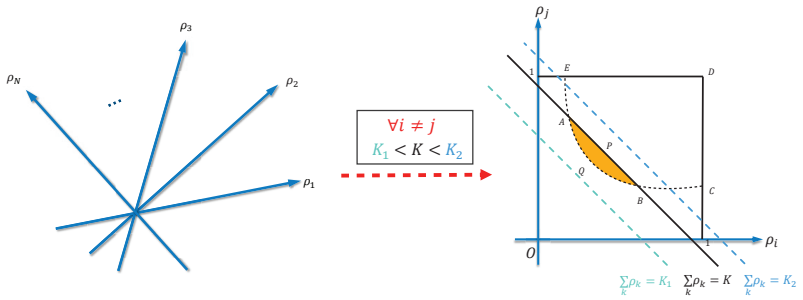

Fig. 2: The feasible zone for $\mathcal{P}_3$ is indicated by the yellow shading. By increasing the parameter K from K_1 to K_2, the previously infeasible problem becomes feasible.

$\boldsymbol{\rho}_2$, it holds that $\mathbf{G}_1\mathbf{A} \leq \mathbf{G}_2\mathbf{A}$ (The symbol $\geq$ is defined in Appendix C). Consequently, based on [29, Corollary 1.5 p-27], we have $\sigma(\mathbf{G}_1\mathbf{A}) \leq \sigma(\mathbf{G}_2\mathbf{A})$.

Based on these two characteristics, we illustrate how K affects the set $\hat{\mathcal{Y}}$ using Fig. 2. As seen in the figure, the left side displays the N dimensions of the variable $\boldsymbol{\rho}$ and the right side illustrates the slice of set $\hat{\mathcal{Y}}$ cut by the plane determined by any two dimensions of $\boldsymbol{\rho}$, i.e. $\rho_i O \rho_j, \forall i \neq j$. Given reasonable $\mathbf{d}, \mathbf{H}$, the zone $EAQBCD$ is non-empty, which denotes the slice of the set $\mathcal{Y}$. The dashed curve $EAQBC$ denotes the boundary on which $\sigma(\mathbf{GA}) = 1$. The line AB denotes the boundary on which $\boldsymbol{\rho}^T\mathbf{1} = K$. The yellow shadow with its boundaries, i.e. $AQBP$, is the slice of the set $\hat{\mathcal{Y}}$, which denotes the slice of the feasible zone cut.

When K is small, i.e. $K = K_1$, the zone $AQBP$ is $\emptyset$, denoting the infeasibility of $\mathcal{P}_3$. However, by increasing K to K_2, the line AB will move parallel to the direction of vector $\vec{OD}$, which would result in the feasibility of the problem. Thereby, we complete the proof. ■

Lemma 4: The total consumed energy $L(\boldsymbol{\rho})$ is monotonically decreasing with respect to the variable $\boldsymbol{\rho} \in \hat{\mathcal{Y}}$.

Proof: The proof is in Appendix E. ■

***Theorem** 4:* The system achieves minimal energy consumption when all available beams are active within the time window; furthermore, increasing the maximum number of simultaneously active beams further reduces the energy consumed.

Proof: The proof is in Appendix F. ■

Theorem 4 demonstrates that the solution to $\mathcal{P}_3$, if it exists, will be located on the boundary where $\boldsymbol{\rho}^T\mathbf{1} = K$. This theorem also suggests that increasing the maximum number of active beams reduces energy consumption. It is important to note that there is an inherent constraint on K, which must not exceed the total number of beams due to the satellite hardware constraints. Choosing an appropriate value for K is a complex task that involves considerations such as size, weight, power (SWaP), and the distribution of traffic demands. However, these considerations are beyond the scope of this paper.

C. Iterative Optimization of Problem $\mathcal{P}_3$

For solving $\mathcal{P}_3$, we will start by rewriting the spectral radius constraint using its equivalent expression. Then, we will develop a method based on Successive Convex Approximation (SCA) [30] to tackle the resulting problem.

In general, the SCA method addresses a complicated problem by iteratively approximating the function value. When the original problem is convex, SCA can find the global optimum [30]. The objective function can be expressed as

$$L(\boldsymbol{\rho}) = \mathrm{Tr}\{(\mathbf{I} - \mathbf{GA})^{-1}\mathbf{GB}\} \tag{13}$$

where $\mathbf{B} = \mathbf{b} \cdot \mathbf{1}^T$, and $\mathrm{Tr}\cdot$ represents the trace of the matrix. Given $\boldsymbol{\rho}_0$ and subsequently defining $\mathbf{G}_0 = \mathtt{Diag}(\mathbf{g}(\boldsymbol{\rho}_0))$, we approximate inverse matrix $(\mathbf{I} - \mathbf{GA})^{-1}$ using its first-order Taylor expansion with respect to the variable $\mathbf{G}$ [31]. This allows us to approximate the total consumed energy as follows: (at the bottom of this page).

Since $\boldsymbol{\Omega}$ is a diagonal matrix of positive elements, the function $y(\mathbf{z}) = \mathbf{z}^T\boldsymbol{\Omega}\mathbf{z}$ is convex and non-decreasing when $\mathbf{z} \succ \mathbf{0}$. As the function $g(\rho)$ is convex, and following the composition rules outlined in [32], the composite function $L(\boldsymbol{\rho}|\boldsymbol{\rho}_0)$ with respect to the variable $\boldsymbol{\rho}$ is also convex. Furthermore, according to [33], $\sigma(\mathbf{X}) \leq t$ is equivalent to $\sigma(\mathbf{X}) \leq t,\ \sigma(-\mathbf{X}) \leq t$, which is further equivalent to

$$\begin{pmatrix} t\mathbf{I} & \mathbf{X} \\ \mathbf{X}^T & t\mathbf{I} \end{pmatrix} \succeq 0. \tag{14}$$

$$L(\boldsymbol{\rho}|\boldsymbol{\rho}_0) \approx \mathrm{Tr}\{\underbrace{(\mathbf{I} - \mathbf{G}_0\mathbf{A})^{-1}}_{\mathbf{T}}\mathbf{GB} + (\mathbf{I} - \mathbf{G}_0\mathbf{A})^{-1}\mathbf{A}(\mathbf{I} - \mathbf{G}_0\mathbf{A})^{-1}\mathbf{GB}(\mathbf{G} - \mathbf{G}_0)\} \tag{15a}$$

$$= \mathbf{g}^T(\boldsymbol{\rho})\underbrace{\mathtt{Diag}(\mathbf{1}^T\mathbf{TATB})}_{\boldsymbol{\Omega}}\mathbf{g}(\boldsymbol{\rho}) + \underbrace{[\mathbf{1}^T\mathbf{TB} - \mathbf{1}^T\mathbf{TATG}_0\mathbf{B}]}_{\hat{\mathbf{b}}^T}\mathbf{g}(\boldsymbol{\rho}) = \mathbf{g}^T(\boldsymbol{\rho})\boldsymbol{\Omega}\mathbf{g}(\boldsymbol{\rho}) + \mathbf{g}^T(\boldsymbol{\rho})\hat{\mathbf{b}} \tag{15b}$$

By substituting the equivalent expression into the constraint $\sigma(\mathbf{GA}) \leq 1$ in $\mathcal{P}_3$, we obtain the subproblem to be solved at each SCA iteration as follows:

$$\mathcal{P}_4 \begin{cases} \underset{\boldsymbol{\rho}}{\texttt{minimize}} & L(\boldsymbol{\rho}|\boldsymbol{\rho}_0) \\ \texttt{subject to} & (\hat{C}_2): \boldsymbol{\rho}^T\mathbf{1} \leq K, \\ & (\tilde{C}_3): \begin{pmatrix} \mathbf{I} & \texttt{Diag}(\mathbf{g}(\boldsymbol{\rho}))\mathbf{A} \\ \mathbf{A}^T\texttt{Diag}(\mathbf{g}(\boldsymbol{\rho})) & \mathbf{I} \end{pmatrix} \succeq 0, \\ & (C_4): \mathbf{0} \preceq \boldsymbol{\rho} \preceq \mathbf{1}, \end{cases}$$

which is convex and can be efficiently solved using CVX [34]. An overview of the proposed approach for solving $\mathcal{P}_3$ is provided in **Algorithm** 1.

Algorithm 1 INVERSE MATRIX OPTIMIZATION

Initialization $\boldsymbol{\rho}_0 = \mathbf{1}, K, \mathbf{A}, \mathbf{d}, \mathbf{H}, k = 0$
repeat
  if $\sigma(\mathbf{G}_k\mathbf{A}) < 1$ **then**
    Set $k = k + 1$, Update $\boldsymbol{\Omega}, \hat{\mathbf{b}}$
    Solve $\boldsymbol{\rho}_{k+1} = \arg \underset{\boldsymbol{\rho}\in\hat{\mathcal{Y}}}{\texttt{minimize}}\ L(\boldsymbol{\rho}|\boldsymbol{\rho}_k)$
  else
    Return: Infeasible
  end if
until $\frac{\|\boldsymbol{\rho}_{k+1}-\boldsymbol{\rho}_k\|_2}{\texttt{dim}(\boldsymbol{\rho}_k)} \leq 10^{-3}$

D. Computational Complexity

The overall computational complexity of Algorithm 1 scales linearly with the number of outer loop iterations. Given $\boldsymbol{\rho}_0$, the non-symmetric exponential cone optimization of $\mathcal{P}_4$ is solved using CVX [35] with an advanced solver, which employs a primal-dual interior point method with a worst-case computational complexity of $\mathcal{O}((MN)^3)$ [36, 37].

V. SECOND-STAGE: STATISTIC-TO-DETERMINISTIC SOLUTION MAPPING

In this section, we first introduce the method to convert the acquired activation probability into discrete demands. Subsequently, we design the illumination pattern, where beam hopping latency is also considered.

A. Conversion to Discrete Demands

Recall that in the previous section, we obtained the optimal beam activation probability and power. To implement this resource allocation solution in a satellite system, we still need to convert them into deterministic illumination operations. This involves selecting time slots for beam activation and assigning the corresponding power.

We present a rounding scheme that converts the continuous probability into discrete demand in the number of TS. According to Theorem 4, the optimum is located on the boundary where $\boldsymbol{\rho}^T\mathbf{1} = K$. Therefore, the rounding algorithm aims to find an integer point, i.e. the number of selected active TS for all beams, that is not only close to $M\boldsymbol{\rho}$ but also sums up to MK. The rounding scheme is detailed in the **Algorithm** 2.

Algorithm 2 ROUNDING

Input: $\boldsymbol{\rho}^\star$, M, K
The lower bound of the demands $\hat{\mathbf{d}} = \lfloor \boldsymbol{\rho}^\star \cdot M \rfloor$
The residual $\mathbf{o} = \boldsymbol{\rho}^\star \cdot M - \hat{\mathbf{d}}$
Sort the residual $\mathbf{o}$ in descending order and find the index of its first $KM - \mathbf{1}^T\hat{\mathbf{d}}$ elements.
Modify the demands $\hat{\mathbf{d}}$ by adding 1 to the selected indexes of beams.

Recall that the relationship between the optimal power and the corresponding activation probability is a one-to-one mapping. Consequently, by applying the rounding algorithm, the power also needs to be modified given that the beam activation probability changes. Specifically, the modification is expressed as

$$\hat{\boldsymbol{\rho}} = \frac{\hat{\mathbf{d}}}{M}, \quad \hat{\mathbf{p}} = \texttt{Diag}(\hat{\boldsymbol{\rho}}^{-1})(\mathbf{I} - \hat{\mathbf{G}}\mathbf{A})^{-1}\hat{\mathbf{G}}\mathbf{b} \tag{17}$$

where $\hat{\mathbf{d}}$ is the vector of converted discrete demands and $\hat{\mathbf{G}} = \texttt{Diag}(\mathbf{g}(\hat{\boldsymbol{\rho}}))$.

B. Mapping to Deterministic Illumination Pattern

With the required power and discrete demand for all beams, the next step is to design the illumination pattern. This involves choosing specific TS from the entire time window to meet the required number of TS for each beam and assigning the necessary power to them. In a prior study [38], a heuristic method was proposed to randomly assign the demands while satisfying the constraints.

However, as discussed in Section III, the problem reformulation is based on the assumption that we have obtained the optimal solution. In other words, the activation probability denotes the probability of a beam being activated during the BH window of the optimal solution, which minimizes consumed energy while meeting the constraints. We follow the optimal assumption to design the deterministic solution $x_{n,t}, \forall n, t$. Given $(\hat{\mathbf{p}}, \hat{\boldsymbol{\rho}})$, the consumed energy is determinate. In this context, we propose focusing on demand-matching performance while satisfying the constraint of a maximum number of active beams. Specifically, our proposed method penalizes the activation of any two beams simultaneously, aiming to minimize the total penalty while adhering to the constraints.

The penalty $\hat{\mathbf{P}} \in \mathbb{R}^{N\times N}$ defines the relative accumulated interference from one beam to the other. Specifically, the interference from the i-th beam to the j-th beam is defined as

$$\hat{P}_{i,j} = \frac{\iint_{\mathbf{S_j}} |H_{i,k}|^2 \, p_i dx_k \, dy_k}{\iint_{\mathbf{S_j}} |H_{j,k}|^2 \, p_j dx_k \, dy_k} \tag{18}$$

where (x_k, y_k) represents the longitude and latitude of user k which is in the beam j; and $\mathbf{S}_j$ stands for the coverage of beam j which is defined by the beam contour at $-3dB$ from the maximum gain.

Moreover, the operator must also take into account the minimization of the beam-hopping latency when designing

the illumination pattern in practice. In the context of the considered system, beam-hopping latency of the beam refers to the number of times the beam switches from on to off and from off to on in a given time window. Given the required number of active time slots for the beam within a specific time window, latency increases more when the frequency of the switch turning on and off is higher. This increase in latency is due to the multiple operations required across various layers, including but not limited to the physical and MAC layers, which result in additional time consumption.

Based on the above illustration, the goal to avoid the latency increase is equivalent to reducing the total number of switching times of the designed beam pattern, which can be expressed as

$$\sum_{n=1}^{N}\sum_{t=1}^{M-1} \parallel x_{n,t} - x_{n,t+1} \parallel^2 \tag{19a}$$

$$= \sum_{n=1}^{N}\{2\hat{d}_n - x_{n,1}^2 - x_{n,M}^2 - \sum_{t=1}^{M-1} 2x_{n,t}x_{n,t+1}\} \tag{19b}$$

$$= -\mathbf{x}^T\tilde{\mathbf{P}}\mathbf{x} + \text{Const} \tag{19c}$$

where $\mathbf{x}_t = [x_{1,t}, \ldots, x_{N,t}]^T$ is the binary vector indicating the status of all beams at TS t, and $\mathbf{x} = [\mathbf{x}_1^T, \ldots, \mathbf{x}_M^T]^T$. The matrix $\tilde{\mathbf{P}}$ is characterized as a block tridiagonal matrix. When $M = 2$ and $M \geq 3$, its expressions can be given respectively by

$$\tilde{\mathbf{P}} = \begin{bmatrix} \mathbf{I}_N & \mathbf{I}_N \\ \mathbf{I}_N & \mathbf{I}_N \end{bmatrix}_{2N\times 2N} \tag{20a}$$

$$\tilde{\mathbf{P}} = \begin{bmatrix} \mathbf{I}_N & \mathbf{I}_N & \mathbf{0}_N & \ldots & \mathbf{0}_N & \mathbf{0}_N \\ \mathbf{I}_N & \mathbf{0}_N & \mathbf{I}_N & \ldots & \mathbf{0}_N & \mathbf{0}_N \\ \mathbf{0}_N & \mathbf{I}_N & \mathbf{0}_N & \ddots & \vdots & \vdots \\ \vdots & \vdots & \ddots & \ddots & \mathbf{I}_N & \mathbf{0}_N \\ \mathbf{0}_N & \mathbf{0}_N & \ldots & \mathbf{I}_N & \mathbf{0}_N & \mathbf{I}_N \\ \mathbf{0}_N & \mathbf{0}_N & \ldots & \mathbf{0}_N & \mathbf{I}_N & \mathbf{I}_N \end{bmatrix}_{MN\times MN} \tag{20b}$$

where $\mathbf{I}_N$ signifies the identity matrix and $\mathbf{0}_N$ represents the zero matrix, both of which are of dimensions $N \times N$."

Therefore, the mapping problem is defined as follows:

$$\mathcal{P}_m \begin{cases} \underset{\mathbf{x}}{\texttt{minimize}} & \mathbf{x}^T(\mathbf{P} - \iota\tilde{\mathbf{P}})\mathbf{x} \\ \texttt{subject to} & (C_5): \mathbf{E}_t\mathbf{x} \preceq K \cdot \mathbf{1}_M \\ & (C_6): \mathbf{E}_b\mathbf{x} = \hat{\mathbf{d}} \\ & (C_7): \mathbf{x} \in \{0,\ 1\}^{MN} \end{cases}$$

where $\mathbf{P} = \texttt{Diag}(\hat{\mathbf{P}}, \ldots, \hat{\mathbf{P}}) \in \mathbb{R}^{MN\times MN}$ is the block diagonal penalty matrix and ι is the trade-off factor between the interference penalty and the operation cost.

The matrix $\mathbf{E}_t = \mathbf{I}_M \otimes \mathbf{1}_N^T$ serves as the selective matrix, with each row selecting all the active beams at TS t, where $\otimes$ denotes the Kronecker product; and $\mathbf{1}_N$ denotes a column vector of dimension N with all elements equal to 1. Additionally, $\mathbf{E}_b = \mathbf{1}_M^T \otimes \mathbf{I}_N$ is another selective matrix, with each row selecting all the active TS for the beam. Lastly, $\hat{\mathbf{d}}$ is the converted discrete demands in terms of the number of TS.

$\mathcal{P}_m$ is a binary quadratic programming (BQP) task, efficiently addressed using the multiplier penalty and majorization-minimization (MPMM) method proposed in our previous work [14].

In summary, Fig. 3 illustrates the procedures of the proposed framework. Given the request demands $\mathbf{d}$, the framework provides the designed illumination pattern $\mathbf{x}$ and the corresponding power of beams $\hat{\mathbf{p}}$ such that the provided capacity $\mathbf{c}$ matches the demands as closely as possible. The preprocessing demand compensation part will be explained in Section VI-C.

TABLE II: Summary of System Parameters

Satellite orbit	13°E (GEO)
Additional payload loss	2 dB
Number of virtual beams (N)	67
Beam radiation pattern ($G_n^{Tx}(x_k, y_k)\, e^{j\phi_{n,k}}$)	Provided by ESA
Downlink carrier frequency	19.5 GHz
User link bandwidth, (B)	500 MHz
Roll-off factor	20%
Temperature	50 K
Number of TSs (M)	20

VI. Numerical Results

In this section, we conduct various simulations to evaluate the proposed framework. First, we demonstrate the influence of system parameters on the final performance. Specifically, we show the convergence of the proposed solving method and validate the theoretical findings. Second, the ideal capacity given by the Shannon formula [39] is undermined in practical implementations, we propose a preprocessing scheme to compensate in advance the difference between the ideal and practical capacities. Third, we analyze the impact of different latency trade-off factors on system-level performance. Lastly, to assess the performance of the proposed framework, we compare it with state-of-the-art alternatives in terms of energy consumption and demand-matching performance, also providing computational time complexity.

A. Simulation Setup

The parameter settings of the GEO satellite are summarized in TABLE II. The traffic demands of all beams are randomly generated and follow a uniform distribution between $400r$ and $1500r$ ($Mbps$), that is, $400r \leq d_n \leq 1500r,\ \forall n$. Herein r stands for the demand density factor, selected from the set $\{0.1, 0.2, 0.3, 0.4, 0.5\}$. For each selected r, 50 demand instances are generated for testing. A single user in the beam center is assumed. To the best of our knowledge, the method described in [14] represents the state-of-the-art and is thus chosen as the baseline. For the baseline, we set the power of each beam as 60 W with 3 dB output back-off (OBO). [1] Unless stated otherwise, all the parameter settings are applied to simulations.

[1]The first step of the baseline is to convert the demands in *bps* into demands in the number of time slots by approximation, within which the expected interference from adjacent beams will be omitted because of the use of precoding. Since there is no precoding in this paper, we would not take this part into account when conducting approximation in the baseline.

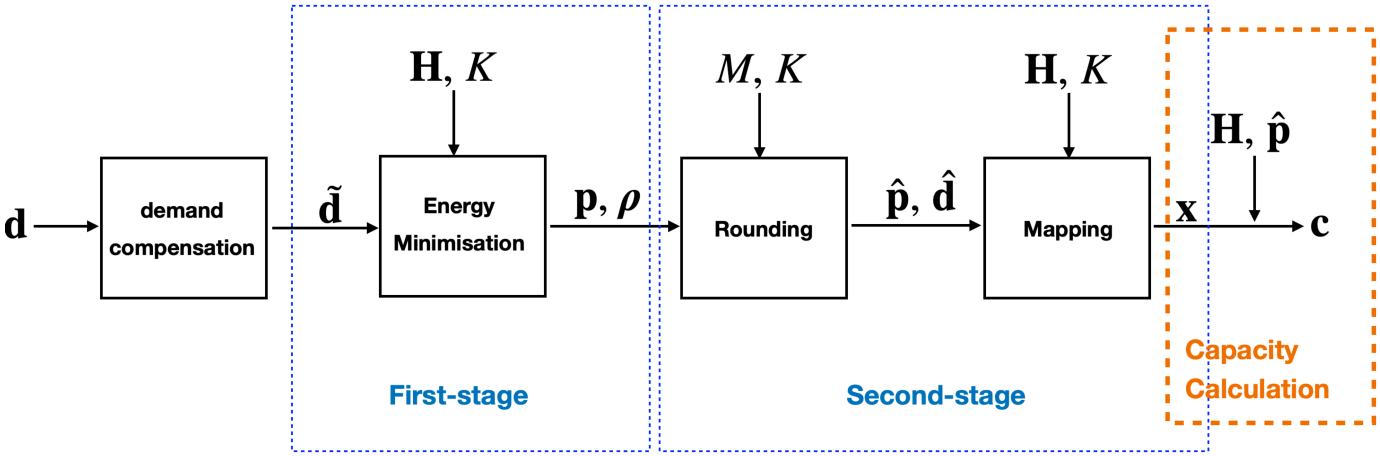

Fig. 3: The proposed framework.

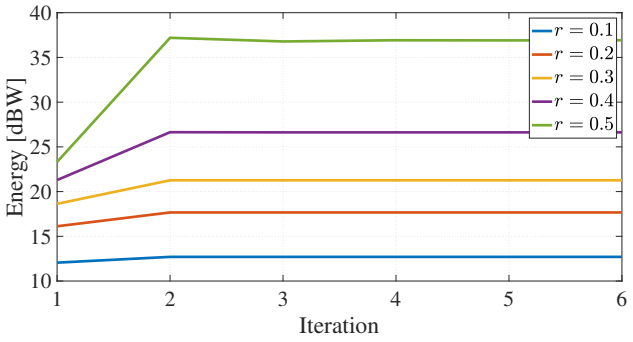

Fig. 4: The convergence of the proposed method. The maximal number of simultaneously active beams $K = 26$, and consumed energy is calculated by $10\log 10(\boldsymbol{\rho}^T\mathbf{p})$.

TABLE III: Influence of K on energy

	$r=0.1$	$r=0.2$	$r=0.3$	$r=0.4$	$r=0.5$
$K=10$	14.89	24.43	NaN	NaN	NaN
$K=15$	13.69	20.34	27.46	NaN	NaN
$K=20$	13.12	18.77	23.43	39.74	NaN
$K=25$	12.80	17.91	21.71	27.87	NaN
$K=30$	12.58	17.37	20.72	25.34	30.80
$K=35$	12.43	17.00	20.07	23.96	27.55
$K=40$	12.32	16.73	19.60	23.07	25.93
$K=45$	12.23	16.52	19.25	22.44	24.90
$K=50$	12.16	16.36	19.00	21.97	24.21

[1] NaN represents that there is no optimal solution in the case.
[2] The energy is given by $10\log 10(\boldsymbol{\rho}^T\mathbf{p})$

TABLE IV: Influence of K on spectral radius

	$r=0.1$	$r=0.2$	$r=0.3$	$r=0.4$	$r=0.5$
$K=10$	0.097	0.477	NaN	NaN	NaN
$K=15$	0.075	0.265	0.644	NaN	NaN
$K=20$	0.066	0.201	0.417	0.970	NaN
$K=25$	0.062	0.171	0.326	0.669	NaN
$K=30$	0.059	0.155	0.278	0.530	0.801
$K=35$	0.057	0.144	0.249	0.452	0.655
$K=40$	0.056	0.136	0.230	0.402	0.567
$K=45$	0.055	0.131	0.216	0.369	0.511
$K=50$	0.054	0.128	0.207	0.346	0.474

[1] NaN represents that there is no optimal solution in the case.
[2] The spectral radius is $\sigma(\mathbf{GA})$ of the optimal solution.

B. Performance of the Proposed Method

1) Convergence of Algorithm 1: Fig. 4 shows the convergence of the proposed Inverse Matrix Optimization Algorithm 1 at different demand densities. As observed, the algorithm converges to the optimum within approximately two to three iterations across all demand densities. We set the initial point to $\boldsymbol{\rho}_0 = \mathbf{1}$, representing the largest value of $\boldsymbol{\rho}$, which results in the minimal objective value and the spectral radius of the matrix. However, this initial point falls outside the feasible zone unless $K = N$. Consequently, the consumed energy initially increases due to the objective function's monotonically decreasing nature.

2) Impact of the maximum number of simultaneously active beams: TABLE III and IV illustrate the influence of the maximum number of simultaneously active beams, denoted as K, on the total consumed energy and the corresponding optimal spectral radius of the matrix $\mathbf{GA}$, respectively.

The results yield the following findings and corresponding analysis: As shown in TABLE III, the total consumed energy decreases with an increase in the maximum number of simultaneously active beams across all demand densities. This observation validates Theorem 4. Furthermore, we confirm *Lemma* 3. Specifically, $\mathcal{P}_3$ becomes feasible when the value of K surpasses a certain threshold. For instance, at a demand density of $r = 0.4$, $\mathcal{P}_3$ is infeasible with the initially set K, but becomes feasible when K is increased to 20. Lastly, comparing TABLE III with TABLE IV, we find that energy consumption has a positive correlation with the spectral radius of the matrix.

3) Correlation among Parameters Density Distribution: We define the parameter density distribution as the normalized distribution of the parameter of the beam across all beams. Fig. 5 intuitively demonstrates the correlation among the density distribution of parameters such as demands, power, activation probability, and consumed energy.

Initially, the given demands are decomposed into power and activation probability with the proposed framework. Subsequently, the consumed energy can be calculated by multiplying the power by the activation probability. As expected, the resulting energy density distribution has great similarity with

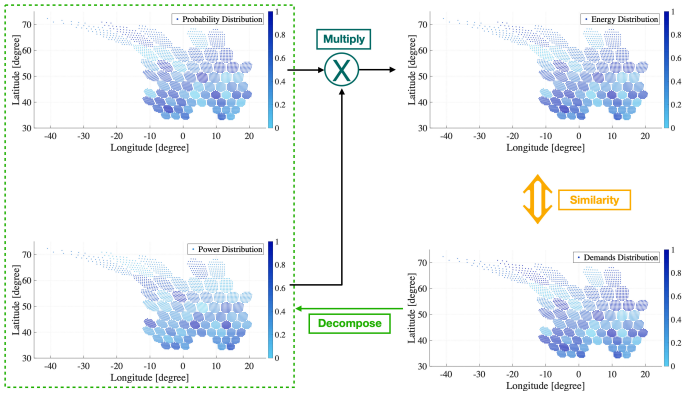

Fig. 5: Density distribution of parameters of an instance. The demand density is at $r = 0.3$.

the given demands density distribution, which validates our proposed framework. Surprisingly, we also find that the probability density distribution has a positive correlation with that of the demands, which suggests an efficient heuristic approach to allocate the limited maximal number of simultaneously active beams.

C. Demand Precompensation

As illustrated in Fig. 3, the proposed two-stage framework aims to design power $\hat{\mathbf{p}}$ and illumination pattern $\mathbf{x}$ for the satellite communication system such that the satellite's capacities (outputs, $\mathbf{c}$) for the ground users match correspondingly the required traffic demands (inputs, $\mathbf{d}$) of these users. In the first stage of the proposed framework, the formulated problem is conditioned on the Shannon Formula, which indicates that the capacity y and the SINR (x) are related by $y = \log_2(1+x)$ as shown in the blue curve in Fig. 6(a).

However, in practice, the operator modulates the signal based on the range of the SINR following the DVB-S2X standard [23] when transmitting the information. Due to these modulations, there is a gap between the Shannon capacity and the DVB-S2X actual output, as seen clearly in Fig. 6(a). Taking a step further, we plot the ratio of DVB-S2X output to Shannon capacity along with SINR, which is the blue curve in Fig. 6(b). It is observed that the information transmission can be conducted well only when the SINR exceeds a particular level. Specifically, when the SINR exceeds 5 dB, the observed ratio surpasses 0.8. However, as long as the ratio is not 1, there is always a transmission loss systematically.

To compensate for the gap, a straightforward approach is to increase the input demands. This adjustment can be expressed as $\tilde{\mathbf{d}} = \mathbf{d}/\epsilon$, where ϵ is the chosen compensation coefficient. With a smaller coefficient, the required demands become higher, resulting in increased energy consumption.

For performance comparison of energy consumption and demand-matching, we choose three different coefficients. The performance metric of energy ratio is defined as

$$\mathrm{ER}_1 = \frac{\boldsymbol{\rho}_\epsilon^{\star T}\mathbf{p}_\epsilon^\star}{\boldsymbol{\rho}_1^{\star T}\mathbf{p}_1^\star} \tag{22}$$

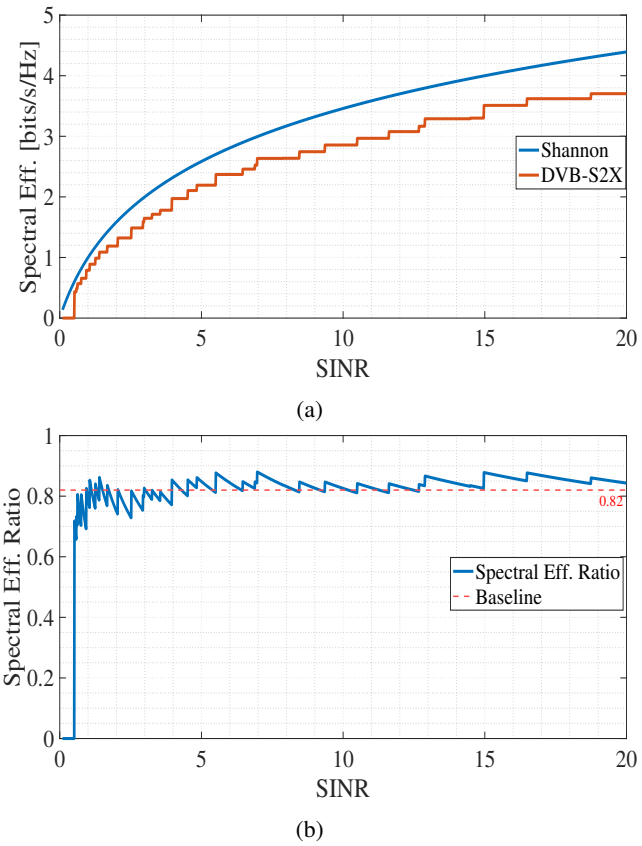

Fig. 6: The comparison between Shannon and DVB-S2X standard in terms of spectral efficiency. (a) the spectral efficiency of DVB-S2X standard and Shannon capacity; (b) the ratio of DVB-S2X standard output to Shannon capacity.

where $\boldsymbol{\rho}_1^\star$ and $\mathbf{p}_1^\star$ are the optimal solutions to $\mathcal{P}_3$; $\boldsymbol{\rho}_\epsilon^\star$ and $\mathbf{p}_\epsilon^\star$ are the compensated ones with the parameter ϵ. While the performance metric of demand matching is illustrated by the cumulative distribution function (CDF) of the ratio of the provided capacity to the required demand (C/D) of the beam.

In Fig. 7(a), the performance of energy ratio is provided. It is observed that the proposed system would necessitate approximately 2.2 times the energy of the ideal system when $\epsilon = 0.80$, whereas it is around 1.8 times when $\epsilon = 0.84$.

Fig. 7(b) demonstrates demand matching performance with different compensation coefficients. The red dashed line indicates the ideal situation where the provided capacity perfectly matches the demand for all beams. It is observed that when $\epsilon = 0.80$, the demands of almost all beams are satisfied. However, with $\epsilon = 0.84$, more than 10% of the beams remain unsatisfied. Additionally, at $\epsilon = 0.82$, less than 5% of the beams are unsatisfied, with the satisfaction ratio ranging between 0.95 and 1. Based on the performance metrics shown in Fig. 7, we conclude that the selection of ϵ represents a trade-off between energy consumption and demand-matching performance. For all subsequent simulations, we will use $\epsilon = 0.82$.

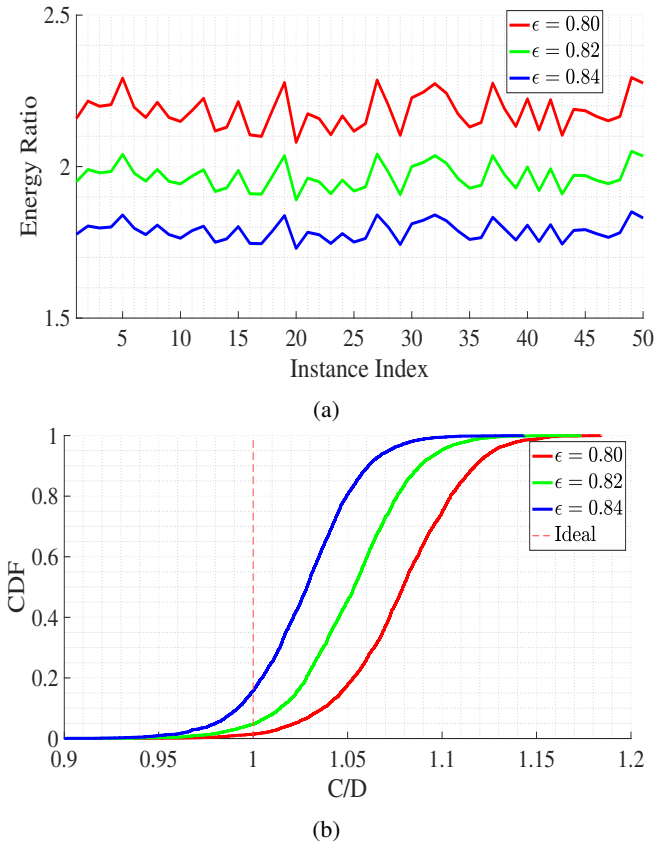

Fig. 7: Performance comparison with different compensation coefficients for the experiment on 50 instance with $r = 0.3$ and the value of K decided via the baseline [14]. (a) energy consumption performance; (b) demand matching performance.

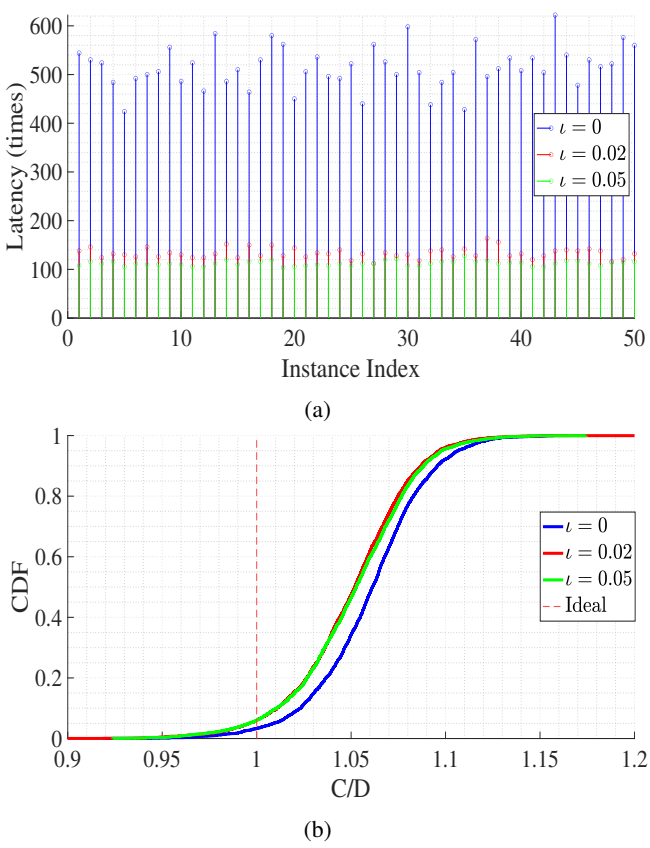

Fig. 8: The influence of trade-off factor on the performance. The demand density is at $r = 0.3$. (a) the total latency per instance; (b) the demand matching ratio per beam.

D. Influence on Latency Trade-off Factor

Fig. 8 demonstrates the influence of the trade-off factor ι on the BH pattern design. Fig. 8(a) examines its impact of three factors on total latency at a demand density $r = 0.3$ across 50 instances. It is shown a significant reduction in latency when the trade-off factor exceeds 0. Moreover, as expected, the larger the factor, the lower the latency. Fig. 8(b) highlights the corresponding demand-matching performance. It is evident that, despite a latency penalty, all three curves of the demand-matching ratio fall within the range of 0.95 and 1.15, demonstrating the superior demand-matching performance of the proposed method. Additionally, as expected, the curve without latency penalties outperforms the latency-penalized curves. Specifically, fewer than 3% of the beams represented by the non-latency-penalized curve fail to meet the criteria, compared to over 6% of the beams depicted by the latency-penalized curve.

E. Designed Illumination Pattern

Fig. 9 shows an example of an illumination pattern designed by the proposed method at a particular demand instance obtained by $r = 0.3$. In Fig. 9(a), the white block refers to the corresponding active beams while the dark ones are passive. Moreover, the beam pattern corresponding to the first TS of the illumination pattern is illustrated in Fig. 9(b), where the green circle refers to the illuminated spot-beam.

F. Influence of Length of Time Window

The influence of the length of time window on the performance is also provided. We define the energy consumption performance metric as

$$\mathrm{ER}_2 = \frac{\hat{\boldsymbol{\rho}}^T \hat{\mathbf{p}}}{\boldsymbol{\rho}^{\star T} \mathbf{p}^\star} \tag{23}$$

where $\boldsymbol{\rho}^\star$ and $\mathbf{p}^\star$ denotes the optimal solution to $\mathcal{P}_3$, and $\hat{\boldsymbol{\rho}}$ and $\hat{\mathbf{p}}$ are the modified solutions obtained after rounding, defined by Eq. (17).

In Fig. 10(a), we can find that the higher the number of time slots (M) in the time window, the closer the distance between the approximated solution and the optimum. For instance, when M is small, i.e. $M = 10$, the total consumed energy increases by a maximum of 8% compared to the optimum. However, when M exceeds 20, the extra required energy stabilizes at less than 1.5% of the optimum. Notably, this amount drops to less than 0.5% when M exceeds 40. Fig. 10(b) illustrates the demand-matching performance. As observed in the figure, almost 10% of beams are not satisfied when $M = 10$, but more than 97% of beams are satisfied when M exceeds 20. Furthermore, the higher the M is, the better the demand-matching performance.

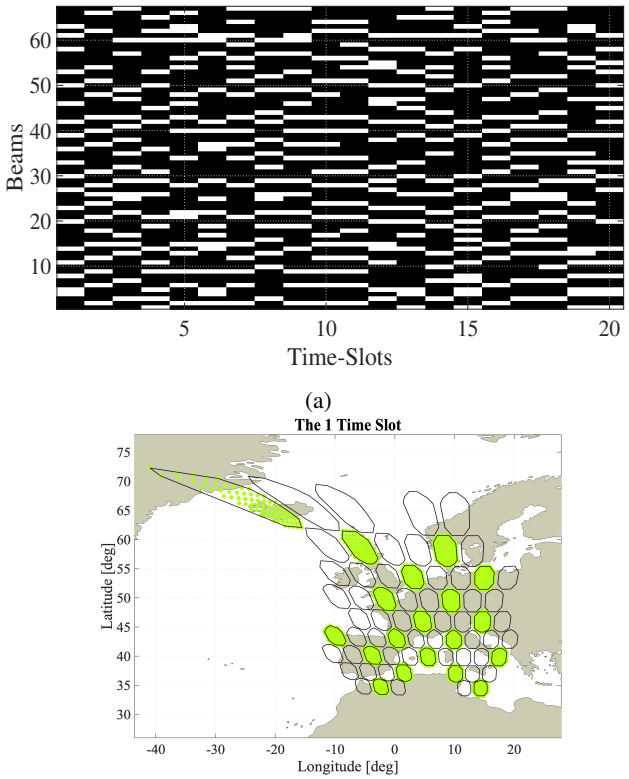

Fig. 9: The designed illumination pattern. (a) illumination pattern; (b) the specific beam pattern at one TS

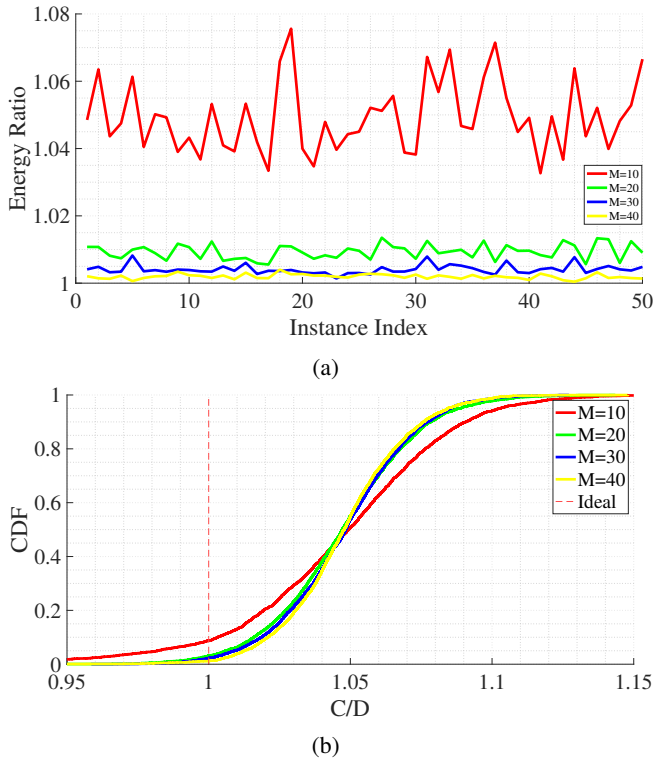

Fig. 10: The influence of M on the performance for the experiments on 50 instances with $r = 0.3$, $K = 21$ and $\epsilon = 0.82$. (a) the energy consumption ratio; (b) the demand matching

G. Comparison with the Baseline on Energy Efficiency and Demand Matching

Fig. 11 demonstrates the performance comparison with the baseline on energy consumption and demand matching across three different demand densities. The performance metric of energy consumption is ER_2 defined by Eq. (23) and the demand matching is by illustrating the CDF of the ratio of the provided capacity to the required demand of the beam. To ensure a fair comparison, both methods are constrained by the same value of K, determined by the method in baseline.

The left-hand side of the figures depict the energy consumption performance. It is evident that the baseline method incurs significantly higher energy costs in all instances, amounting to approximately 2.5 times, 1.5 times, and 1.2 times the energy consumed by the proposed framework at demand densities $r = 0.1, 0.3, 0.5$, respectively. The right-hand side figures illustrate the demand-matching performance. Although the baseline successfully fulfills the requirements for nearly all beams, it tends to exceed the necessary capacity. In contrast, the proposed method demonstrates greater stability in its performance. The demand-matching ratio generally falls within the range of 0.95 to 1.1 across all demand densities.

H. Comparison with Baseline on Computational Complexity

Fig. 12 presents the time consumption of the proposed framework relative to the baseline at the different number of variables. The y-axis value is the ratio of the time consumption of the proposed framework to that of the baseline, which is averaged over 50 instances at $r = 0.3$, $M = 20$. The number of variables is MN, where $N \in \{10, 20, 30, 40, 50, 60, 67\}$ is the number of beams and M is the number of TS in the time window. The convergence conditions of the iterative algorithms are given by $\frac{\|\mathbf{x}_{k+1}-\mathbf{x}_k\|_2}{\texttt{dim}(\mathbf{x}_k)} \leq 10^{-3}$, where $\texttt{dim}(\mathbf{x})$ denotes the dimension of the vector $\mathbf{x}$.

We also provide Table V, which compares the system performances of the proposed framework and the baseline. The Jain's Fairness Index is used to measure the satisfaction coverage of the users' demands and is defined as $f(\mathbf{y}) = \frac{(\sum_i y_i)^2}{\texttt{dim}(\mathbf{y}) \sum_i y_i^2)}$, where the merit function $y_i = \frac{c_i}{d_i}$ is the ratio of the provided capacity to the request traffic demand of the beam [40]. The higher the index is, the better the scheme of the resource allocation would be. In addition, statistical parameters for the energy consumption ratio of the proposed framework to that of the baseline across 50 instances are also provided. Based on the results, we can see that, although the running time of the proposed framework is around 1.3 times that of the baseline, the system gets a notable performance improvement. Specifically, the proposed solution consumes only 65% of the energy by the baseline while still providing slightly better demand-matching performance.

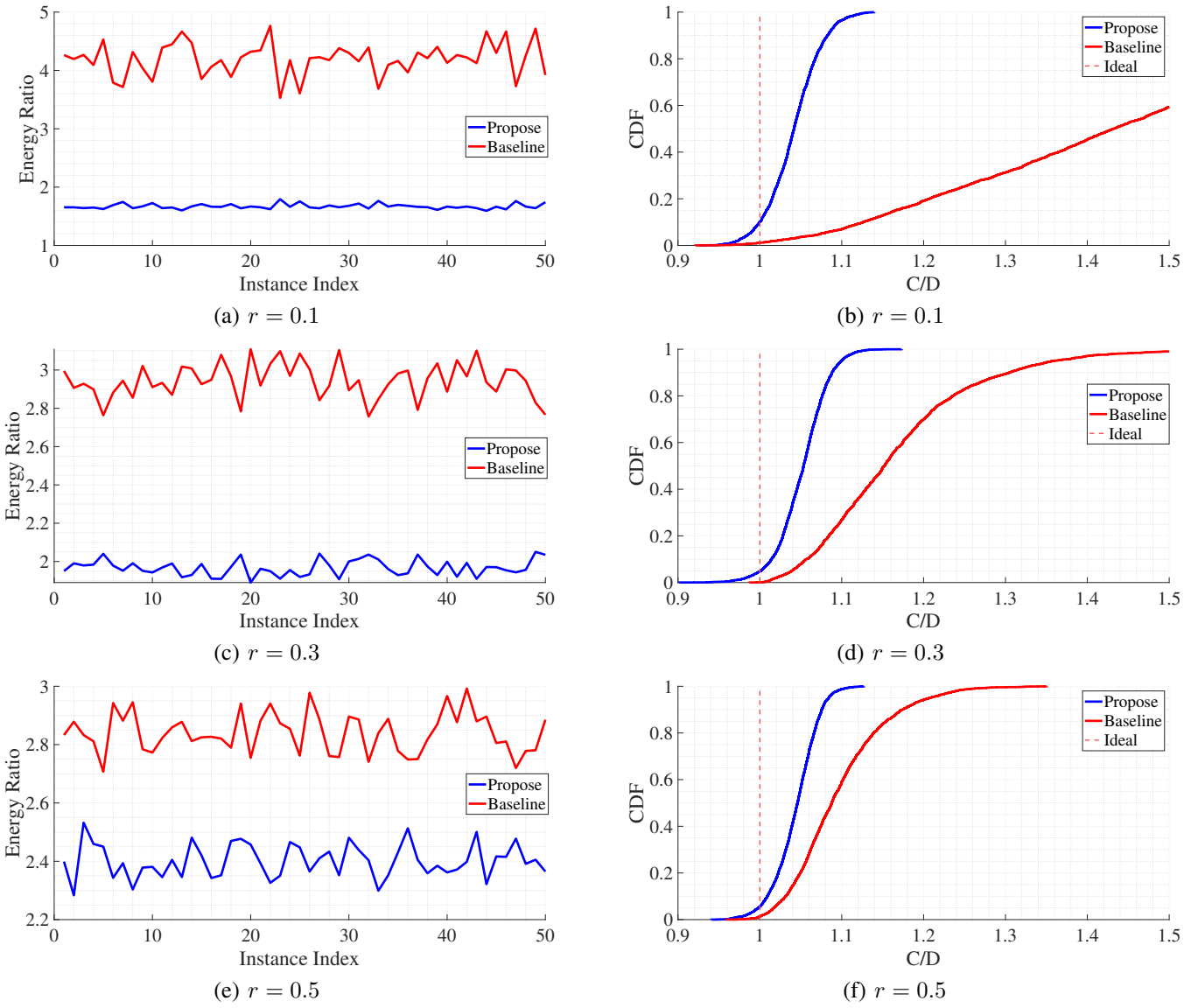

(a) $r = 0.1$ (b) $r = 0.1$

(c) $r = 0.3$ (d) $r = 0.3$

(e) $r = 0.5$ (f) $r = 0.5$

Fig. 11: The performance comparison between the proposed method with the baseline.

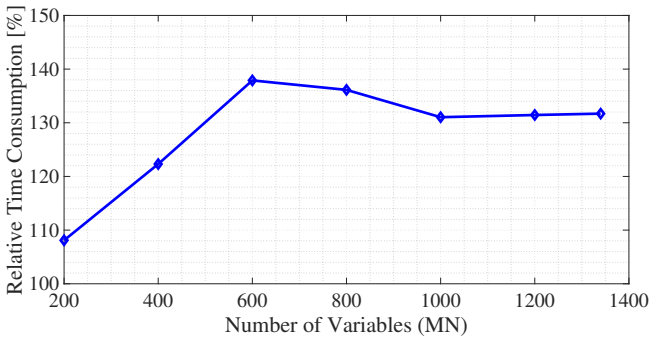

Fig. 12: The relative time-consumption comparison.

VII. Conclusion

In this paper, we propose a novel two-stage framework for optimizing energy consumption through the joint design of power and time slot allocation. The framework is designed to achieve optimal performance by addressing various challenges. In the first stage, we utilize mean-field theory to extract the activation probability and reformulate the mathematical model into an inverse matrix optimization problem. This reformulation enables us to convert the problem into a convex form, which has been thoughtfully analyzed and solved efficiently using a proposed iterative method. In the second stage, we employ the MPMM method to map the activation probability into the illumination pattern. Additionally, we introduce a compensation method to mitigate the performance loss resulting from the discrepancy between practical adaptive coding modulation and the ideal Shannon formula. Overall, this step yields a deterministic and practical solution for the considered beam-hopping satellite system. To validate our theoretical findings, we conduct numerical simulations. The results demonstrate that our proposed method surpasses the benchmark in terms of energy consumption and demand-matching performance.

TABLE V: Performance comparison on resource allocation fairness and total consumed energy

	Number of Variables	200	400	600	800	1000	1200	1340
Jain's Fairness Index	Proposed	0.9994	0.9992	0.9992	0.9992	0.9991	0.9991	0.9990
	Baseline	0.9898	0.9904	0.9909	0.9920	0.9925	0.9930	0.9922
Consumed Energy	Mean	0.5119	0.6333	0.6159	0.6444	0.6647	0.6739	0.6766
	Min	0.3744	0.4839	0.5295	0.5608	0.5730	0.6125	0.6073
	Max	0.7931	0.8026	0.7801	0.7535	0.7564	0.7602	0.7583

[a] "Consumed Energy" denotes the ratio of energy consumption of the proposed framework to that of the baseline.

APPENDIX A

Proof: Given $\mathbf{d}, \mathbf{H}$, and K, assume that the optimal solution to $\mathcal{P}_1$ is $(\boldsymbol{\rho}^\star, \mathbf{p}^\star)$. Consequently, this solution satisfies the demand constraint $\hat{C}_2$.

Suppose $(\boldsymbol{\rho}^\star, \mathbf{p}^\star)$ is not the fixed point, taking into account that it is the solution to the problem into account, then there $\exists n$ such that $\rho_n^\star > f_n(\boldsymbol{\rho}^\star, \mathbf{p}^\star)$ and $\rho_i^\star \geq f_i(\boldsymbol{\rho}^\star, \mathbf{p}^\star),\ \forall i \neq n$. Consequently, there exists another point $(\hat{\boldsymbol{\rho}}, \mathbf{p}^\star)$ such that $\hat{\rho}_n = f_n(\boldsymbol{\rho}^\star, \mathbf{p}^\star)$ and $\hat{\rho}_i = \rho_i^\star,\ \forall i \neq n$. Subsequently, according to the definition at Eq. (6), there would have $\hat{\rho}_i > f_i(\hat{\boldsymbol{\rho}}, \mathbf{p}),\ \forall i \neq n$, which proves that it is the feasible solution to the problem. Moreover, it consumes less energy than the supposed optimal solution, which contradicts the optimal assumption. Thus the optimal solution to $\mathcal{P}_1$ should be the fixed point of the equations. ∎

APPENDIX B

Proof: The first-order and second-order derivatives of the function $g(z)$ are given by $g^{'}(z) = 2^{\frac{d}{Bz}}(1 - \frac{d\ln 2}{Bz}) - 1$ and $g^{''}(z) = \frac{1}{z^3}\frac{(d\ln 2)^2}{B^2}2^{\frac{d}{Bz}}$ respectively. There always holds that $g^{''}(z) > 0, \forall z > 0$, so the first-order derivative of the function is monotonically increasing on the zone $(0, +\infty)$. Taking $g^{'}(+\infty) = 0$ into account, we would have $g^{'}(z) < 0, \forall z > 0$ and thereby completes the proof.

∎

APPENDIX C

Proof: We define the given parameters are reasonable if the minimal spectral radius of the matrix is no greater than 1. If the condition is not met, the parameters are irreasonable. When given irreasonable parameters $\mathbf{H}, \mathbf{d}$, the set is empty, i.e. $\mathcal{Y} = \emptyset$, thus it is convex. In the following, we will first give the condition to check if the given parameters are reasonable, and then prove the convexity of the set when given reasonable parameters.

Firstly, we define $\mathbf{A} \geq \mathbf{B}$ if $A_{i,j} \geq B_{i,j},\ \forall i, j$, and $\mathbf{A} > \mathbf{B}$ if $\mathbf{A} \geq \mathbf{B},\ \mathbf{A} \neq \mathbf{B}$. According to [29, Corollary 1.5 on p.27], given matrix $\mathbf{A}, \mathbf{B}$, if $\mathbf{A} > \mathbf{B} > \mathbf{0}$, there would have $\sigma(\mathbf{A}) > \sigma(\mathbf{B})$, where $\mathbf{0}$ is the matrix all of whose elements are 0. Moreover, based on the *Lemma* 4, the function $g(z)$ is monotonically decreasing, thus the minimal spectral radius of the matrix $\mathbf{GA} = \mathtt{Diag}(\mathbf{g}(\boldsymbol{\rho}))\mathbf{A}$ is at the point $\boldsymbol{\rho} = \mathbf{1}$ as $\mathbf{1} \succeq \boldsymbol{\rho} \in \mathcal{Y}$. According to the previous definition, the condition is to check if the spectral radius of the matrix $\mathtt{Diag}(\mathbf{g}(\mathbf{1}))\mathbf{A}$ is less than 1.

Secondly, when given reasonable parameters, the set $\mathcal{Y}$ is non-empty. Suppose $\boldsymbol{\rho}_1, \boldsymbol{\rho}_2 \in \mathcal{Y}$, then there have $\sigma(\mathbf{G}_1\mathbf{A}) \leq 1, \sigma(\mathbf{G}_2\mathbf{A}) \leq 1$, where $\mathbf{G}_i = \mathtt{Diag}(\mathbf{g}(\boldsymbol{\rho}_i)),\ i = 1, 2$.

Assume that $\boldsymbol{\rho} = \theta\boldsymbol{\rho}_1 + (1-\theta)\boldsymbol{\rho}_2, \forall\ \theta \in [0\ 1]$. According to [41, Remark 1.3], if the function $g(z)$ is log-convex, there would have $\sigma(\mathbf{GA}) \leq \sigma(\mathbf{G}_1\mathbf{A})^\theta \cdot \sigma(\mathbf{G}_2\mathbf{A})^{(1-\theta)} \leq 1$, which proves that the convexity of the set is conditioned on the log-convex of the function $g(z)$. In the following, we will prove the log-convex of the function $g(z)$.

According to [35], that a function is log-convex is equivalent to the positivity of the function $h(z) = g(z)\cdot g(z)^{''} - (g(z)^{'})^2$. The function $h(z)$ and its first-order derivative can be given by $h(z) = (t^2-t)\frac{m^2}{z^2} - [t(1-m)-1]^2$ and $h^{'}(z) = \frac{m^2}{z^3}\{2t^2m(z^2-1)+t(m-4t)+z^2(2t-2t^2)\}$ respectively, where $t = 2^{\frac{d}{Bz}}, m = \frac{d\ln 2}{Bz}$. Considering that there would have $(z^2-1) \leq 0, (m-4t) < 0, (2t-2t^2) < 0,\ \forall\ 0 < z \leq 1$, subsequently $h^{'}(z) < 0$, which proves that the function $h(z)$ is strictly decreasing. Taking into account that $h(\infty) = 0$, thus $\forall z > 0, h(z) > 0$. According to [35], the function $g(z)$ is log convex, which thereby completes the proof.

∎

APPENDIX D

Proof: According to *Lemma* 2, the set $\hat{\mathcal{Y}}$ is the intersection of two convex sets, thus it is convex [35]. In the following, we will first prove the convexity of $\mathcal{P}_3$ and then demonstrate that the solutions to $\mathcal{P}_2$ and $\mathcal{P}_3$ are equivalent.

The total derivatives of the objective function $L(\boldsymbol{\rho})$ is given by

$$\mathrm{d}L(\boldsymbol{\rho}) = \mathrm{Tr}\{\mathrm{d}[(\mathbf{I}-\mathbf{GA})^{-1}]\mathbf{GB} + (\mathbf{I}-\mathbf{GA})^{-1}\mathrm{d}[\mathbf{G}]\mathbf{B}\} \tag{24a}$$

$$= \mathrm{Tr}\{\underbrace{(\mathbf{A}(\mathbf{I}-\mathbf{GA})^{-1}\mathbf{GB} + \mathbf{B})((\mathbf{I}-\mathbf{GA})^{-1}}_{\mathbf{Z}}\mathrm{d}[\mathbf{G}]\} \tag{24b}$$

where $\mathbf{B} = \mathbf{b}\cdot\mathbf{1}^T$.

Note that $\mathbf{G} = \mathtt{Diag}(\mathbf{g}(\boldsymbol{\rho}))$ is a diagonal matrix, thus

$$\mathrm{d}[\mathbf{G}] = \mathtt{Diag}([g^{'}(\rho_1)d\rho_1, \ldots, g^{'}(\rho_N)d\rho_N]^T) \tag{25}$$

According to [42] and Eq. (24b, 25), the first-order derivative of the objective $L(\boldsymbol{\rho})$ is

$$\frac{\partial L}{\partial \rho_i} = Z_{i,i}g^{'}(\rho_i),\ \forall i \tag{26}$$

Subsequently the Hessian matrix of the objective is given by $\frac{\partial L^2}{\partial\rho_i\partial\rho_j} = \begin{cases} 0 & i \neq j \\ Z_{i,i}g^{''}(\rho_i) & i = j \end{cases}$, which is a diagonal matrix.

In the following, we will prove the positive of the elements in the diagonal of the matrix. First, according to *Lemma* 1, we have $g^{''}(\rho_i) > 0,\ \forall\rho_i > 0$. Second, when

$\boldsymbol{\rho} \in \hat{\mathcal{Y}} \setminus \{\boldsymbol{\rho} | \sigma(\mathbf{GA}) = 1\}$, there have $(\mathbf{I} - \mathbf{GA})^{-1} \succ \mathbf{0}$ because of $\sigma(\mathbf{GA}) < 1$. Then, according to the definition of $\mathbf{Z}$ in (24b), there have $Z_{i,i} > 0 \ \forall i$. Taking these two parts into account, the Hessian matrix of the objective is positive definite at the domain $\boldsymbol{\rho} \in \hat{\mathcal{Y}} \setminus \{\boldsymbol{\rho} | \sigma(\mathbf{GA}) = 1\}$. In addition, when $\boldsymbol{\rho} \in \{\boldsymbol{\rho} | \sigma(\mathbf{GA}) = 1\}$, there would have $\lim_{\sigma(\mathbf{GA}) \to 1} L(\boldsymbol{\rho}) = +\infty$. To summarize, $\mathcal{P}_3$ is convex.

The difference between $\mathcal{P}_2$ and $\mathcal{P}_3$ is that the feasible set of $\mathcal{P}_3$ contains the boundary points, i.e. $\boldsymbol{\rho} \in \{\boldsymbol{\rho} | \sigma(\mathbf{GA}) = 1\} \cup \{\mathbf{0}\}$, while $\mathcal{P}_2$ does not. However, the optimum would not be located at these boundaries as $\lim_{\sigma(\mathbf{GA}) \to 1} L(\boldsymbol{\rho}) = +\infty$. Thereby we complete the proof. ∎

APPENDIX E

Proof: According to the Appendix D , the first order derivative of $L(\boldsymbol{\rho})$ is $\frac{\partial L}{\partial \rho_i} = Z_{i,i} g^{'}(\rho_i)$, where $\mathbf{Z} = (\mathbf{A}(\mathbf{I} - \mathbf{GA})^{-1}\mathbf{GB} + \mathbf{B})((\mathbf{I} - \mathbf{GA})^{-1}$. For $\forall \boldsymbol{\rho} \in \hat{\mathcal{Y}}$, there would have $\sigma(\mathbf{GA}) \leq 1$, and thus $Z_{i,i} > 0, \ \forall i$. In addition, according to *Lemma* 1, $g^{'}(z) < 0, \forall z > 0$. To sum up, the first-order derivative of the objective is negative, so the total consumed energy is monotonically decreasing within the feasible zone. ∎

APPENDIX F

Proof: Suppose $\boldsymbol{\rho}^{\star}$, the solution to $\mathcal{P}_3$, is not on the boundary, i.e. $(\boldsymbol{\rho}^{\star})^T \mathbf{1} < K$. Consequently, without losing generality, we can always construct a point $\boldsymbol{\rho}^{+}$ in the following manner: given any index n, the set $\rho_j^{+} = \rho_j^{\star}$, for all $j \neq n$, and $\rho_n^{+} > \rho_n^{\star}$. This configuration also satisfies the condition $(\boldsymbol{\rho}^{+})^T \mathbf{1} = K$.

Because of the monotonically decreasing of the function $g(z)$ and the corollary in [29, Corollary 1.5 p-27], there would have $\sigma(\texttt{Diag}(\mathbf{g}(\boldsymbol{\rho}^{\star}))) > \sigma(\texttt{Diag}(\mathbf{g}(\boldsymbol{\rho}^{+})))$. In addition, taking the constraint $\sigma(\texttt{Diag}(\mathbf{g}(\boldsymbol{\rho}^{\star}))) \leq 1$ into account, there has $\sigma(\texttt{Diag}(\mathbf{g}(\boldsymbol{\rho}^{+}))) < 1$. Consequently, the constructed point is in the feasible set, i.e. $\boldsymbol{\rho}^{+} \in \hat{\mathcal{Y}}$.

However, according to the *Lemma* 4, the objective $L(\boldsymbol{\rho})$ is monotonically decreasing. Thus there would have $L(\boldsymbol{\rho}^{\star}) > L(\boldsymbol{\rho}^{+})$ as $\boldsymbol{\rho}^{\star} \preceq \boldsymbol{\rho}^{+}$. This contradicts the optimal assumption. Therefore, if a solution to $\mathcal{P}_3$ exists, it would be located on the boundary. This implies that the system achieves minimal energy consumption when all available beams are activated simultaneously. With this, we complete the first part of the theorem.

As seen in Fig. 2, the line AB would move parallel to the direction of vector $\vec{OD}$ when K is increased, resulting in the solution of the former preceding the latter, i.e. $\boldsymbol{\rho}_{former}^{\star} \prec \boldsymbol{\rho}_{latter}^{\star}$. Considering that the objective function is monotonically decreasing, we deduce that $L(\boldsymbol{\rho}_{former}^{\star}) > L(\boldsymbol{\rho}_{latter}^{\star})$. This indicates that increasing the maximum number of active beams reduces the consumed energy, thereby completing the proof. ∎

REFERENCES

[1] O. Kodheli, E. Lagunas, N. Maturo, S. K. Sharma, B. Shankar, J. F. M. Montoya, J. C. M. Duncan, D. Spano, S. Chatzinotas, S. Kisseleff *et al.*, "Satellite communications in the new space era: A survey and future challenges," *IEEE Communications Surveys & Tutorials*, vol. 23, no. 1, pp. 70–109, 2020.

[2] G. Araniti, A. Iera, S. Pizzi, and F. Rinaldi, "Toward 6G non-terrestrial networks," *IEEE Network*, vol. 36, no. 1, pp. 113–120, 2022.

[3] G. Cocco, T. De Cola, M. Angelone, Z. Katona, and S. Erl, "Radio resource management optimization of flexible satellite payloads for DVB-S2 systems," *IEEE Transactions on Broadcasting*, vol. 64, no. 2, pp. 266–280, 2017.

[4] G. Taricco and A. Ginesi, "Precoding for flexible high throughput satellites: Hot-spot scenario," *IEEE Transactions on Broadcasting*, vol. 65, no. 1, pp. 65–72, 2019.

[5] A. Freedman, D. Rainish, and Y. Gat, "Beam hopping how to make it possible," in *Proc. of Ka and Broadband Communication Conference, Bologna, Italy*, Oct. 2015.

[6] A. Morello and N. Alagha, "DVB-S2X air interface supporting beam hopping systems," in *25th Ka and Broadband Communications Conference, (Ka-2019), Sorrento, Italy*, Oct. 2019, pp. 1–5.

[7] C. Rohde, D. Rainish, A. Freedman, G. Lesthievent, N. Alagha, D. Delaruelle, G. Mocker, and X. Giraud, "Beam-hopping system configuration and terminal synchronization schemes," in *Proceedings of the 37th International Communications Satellite Systems Conference (ICSSC-2019)*, 2019, pp. 1–13.

[8] T. Posielek, "An energy management approach for satellites," in *69th International Astronautical Congress, Bremen, Germany*, Oct. 2018, pp. 1–5.

[9] C. N. Efrem and A. D. Panagopoulos, "Dynamic energy-efficient power allocation in multibeam satellite systems," *IEEE Wireless Communications Letters*, vol. 9, no. 2, pp. 228–231, 2019.

[10] Y. Yang, M. Xu, D. Wang, and Y. Wang, "Towards energy-efficient routing in satellite networks," *IEEE Journal on Selected Areas in Communications*, vol. 34, no. 12, pp. 3869–3886, 2016.

[11] P. Angeletti, D. F. Prim, and R. Rinaldo, "Beam hopping in multi-beam broadband satellite systems: System performance and payload architecture analysis," in *24th AIAA International Communications Satellite Systems Conference*. [Online]. Available: https://arc.aiaa.org/doi/abs/10.2514/6.2006-5376

[12] A. Ginesi, E. Re, and P. Arapoglou, "Joint beam hopping and precoding in hts systems," in *9th Int. Conf. on Wireless and Satellite Systems (WiSATS)*, 2017.

[13] M. G. Kibria, E. Lagunas, N. Maturo, D. Spano, and S. Chatzinotas, "Precoded cluster hopping in multi-beam high throughput satellite systems," in *2019 IEEE Global Communications Conference (GLOBECOM)*, 2019, pp. 1–6.

[14] L. Chen, V. N. Ha, E. Lagunas, L. Wu, S. Chatzinotas, and B. Ottersten, "The next generation of beam hopping satellite systems: Dynamic beam illumination with selective precoding," *IEEE Transactions on Wireless Communications*, 2022.

[15] L. Lei, E. Lagunas, Y. Yuan, M. G. Kibria, S. Chatzinotas, and B. Ottersten, "Beam illumination pattern design in satellite networks: Learning and optimization for efficient beam hopping," *IEEE Access*, vol. 8, pp. 136 655–136 667, 2020.

[16] Z. Lin, Z. Ni, L. Kuang, C. Jiang, and Z. Huang, "Satellite-terrestrial coordinated multi-satellite beam hopping scheduling based on multi-agent deep reinforcement learning," *IEEE Transactions on Wireless Communications*, 2024.

[17] J. P. Choi and V. W. Chan, "Optimum power and beam allocation based on traffic demands and channel conditions over satellite downlinks," *IEEE Transactions on Wireless Communications*, vol. 4, no. 6, pp. 2983–2993, 2005.

[18] T. S. Abdu, S. Kisseleff, E. Lagunas, and S. Chatzinotas, "Flexible resource optimization for geo multibeam satellite communication system," *IEEE Transactions on Wireless Communications*, vol. 20, no. 12, pp. 7888–7902, 2021.

[19] I. Siomina and D. Yuan, "Analysis of cell load coupling for lte network planning and optimization," *IEEE Transactions on Wireless Communications*, vol. 11, no. 6, pp. 2287–2297, 2012.

[20] C. K. Ho, D. Yuan, L. Lei, and S. Sun, "Power and load coupling in cellular networks for energy optimization," *IEEE Transactions on Wireless Communications*, vol. 14, no. 1, pp. 509–519, 2014.

[21] M. Opper and D. Saad, *Advanced mean field methods: Theory and practice*. MIT press, 2001.

[22] C. M. Bishop and N. M. Nasrabadi, *Pattern recognition and machine learning*. Springer, 2006, vol. 4, no. 4.

[23] D. V. Broadcasting(DVB)Project, "Digital video broadcasting(DVB); second generation DVB interactive satellite system (DVB-S2X)," *ETSI EN 302 307 V1.4.1*, 2019.

[24] C. Rohde, R. Wansch, G. Mocker, A. Trutschel-Stefan, L. Roux,

E. Feltrin, H. Fenech, and N. Alagha, "Beam-hopping over-the-air tests using DVB-S2X super-framing," in *36th International Communications Satellite Systems Conference (ICSSC 2018)*, 2018.
[25] A. I. Perez-Neira, M. A. Vazquez, M. B. Shankar, S. Maleki, and S. Chatzinotas, "Signal processing for high-throughput satellites: Challenges in new interference-limited scenarios," *IEEE Signal Processing Magazine*, vol. 36, no. 4, pp. 112–131, 2019.
[26] A. Granas and J. Dugundji, *Fixed point theory*. Springer, 2003, vol. 14.
[27] W. I. Zangwill, *Nonlinear programming: a unified approach*. Prentice-Hall Englewood Cliffs, NJ, 1969, vol. 52.
[28] C. K. Ho, D. Yuan, and S. Sun, "Data offloading in load coupled networks: A utility maximization framework," *IEEE Transactions on Wireless Communications*, vol. 13, no. 4, pp. 1921–1931, 2014.
[29] A. Berman and R. J. Plemmons, *Nonnegative matrices in the mathematical sciences*. SIAM, 1994.
[30] M. Razaviyayn, M. Hong, and Z.-Q. Luo, "A unified convergence analysis of block successive minimization methods for nonsmooth optimization," *SIAM Journal on Optimization*, vol. 23, no. 2, pp. 1126–1153, 2013.
[31] K. B. Petersen, M. S. Pedersen *et al.*, "The matrix cookbook," *Technical University of Denmark*, vol. 7, no. 15, p. 510, 2008.
[32] M. Grant, S. Boyd, and Y. Ye, "Disciplined convex programming," *Global optimization: From theory to implementation*, pp. 155–210, 2006.
[33] A. Ben-Tal and A. Nemirovski, *Lectures on modern convex optimization: analysis, algorithms, and engineering applications*. SIAM, 2001.
[34] M. Grant and S. Boyd, "CVX: Matlab software for disciplined convex programming, version 2.1," 2014.
[35] S. Boyd, S. P. Boyd, and L. Vandenberghe, *Convex optimization*. Cambridge university press, 2004.
[36] F. Curtis and J. Nocedal, "Steplength selection in interior-point methods for quadratic programming," *Applied mathematics letters*, vol. 20, no. 5, pp. 516–523, 2007.
[37] J. Dahl and E. D. Andersen, "A primal-dual interior-point algorithm for nonsymmetric exponential-cone optimization," *Mathematical Programming*, vol. 194, no. 1-2, pp. 341–370, 2022.
[38] L. Chen, E. Lagunas, L. Lei, S. Chatzinotas, and B. Ottersten, "Adaptive resource allocation for satellite illumination pattern design," in *2022 IEEE 96th Vehicular Technology Conference (VTC2022-Fall)*. IEEE, 2022, pp. 1–6.
[39] C. E. Shannon, "A mathematical theory of communication," *ACM SIGMOBILE mobile computing and communications review*, vol. 5, no. 1, pp. 3–55, 2001.
[40] R. K. Jain, D.-M. W. Chiu, W. R. Hawe *et al.*, "A quantitative measure of fairness and discrimination," *Eastern Research Laboratory, Digital Equipment Corporation, Hudson, MA*, vol. 21, p. 1, 1984.
[41] R. D. Nussbaum, "Convexity and log convexity for the spectral radius," *Linear Algebra and its Applications*, vol. 73, pp. 59–122, 1986.
[42] X.-D. Zhang, *Matrix analysis and applications*. Cambridge University Press, 2017.

Lin Chen received the B.E. degree in acoustics and M.E. degree in acoustic signal processing at the Northwestern Polytechnical University (NPU), Xi'an, China, in 2014 and 2017 respectively (both with honors). He was with Samsung R&D Institute China-Shenzhen as an Algorithm Engineer working on designing transmit chain of base station from 2017 to 2019. Since Sep. 2020, he has been pursuing his Ph.D. degree in telecommunication engineering at the Interdisciplinary Centre for Security, Reliability and Trust (SnT), University of Luxembourg. His research interests are in general areas of signal processing, optimization and machine learning based solution for radio resource management.

Linlong Wu received the B.E. degree in electronic information from Xi'an Jiaotong University (XJTU), Xi'an, China, in 2014, and the Ph.D. degree in electronic and computer engineering from Hong Kong University of Science and Technology (HKUST), Hong Kong, in 2018. From November 2018 to October 2020, he was with the wireless network group of Alibaba Cloud as a Research Engineer working on designing and building commercial RFID-based localization systems. Since November 2020, he has been with the Interdisciplinary Centre for Security, Reliability and Trust (SnT), University of Luxembourg, and he is currently a Research Scientist with the Signal Processing Applications in Radar and Communications (SPARC) Group. His research interests include signal processing, optimization, and machine learning with applications in waveform design, integrated sensing and communication, and IoT networks.

Eva Lagunas (S'09-M'13-SM'18) received the MSc and PhD degrees in telecommunications engineering from the Polytechnic University of Catalonia (UPC), Barcelona, Spain, in 2010 and 2014, respectively. She was Research Assistant within the Department of Signal Theory and Communications, UPC, from 2009 to 2013. In 2009 she was a guest research assistant within the Department of Information Engineering, University of Pisa, Italy. From November 2011 to May 2012 she held a visiting research appointment at the Center for Advanced Communications (CAC), Villanova University, PA, USA. In 2014, she joined the Interdisciplinary Centre for Security, Reliability and Trust (SnT), University of Luxembourg, where she currently holds a Research Scientist position. Her research interests include radio resource management and general wireless networks optimization.

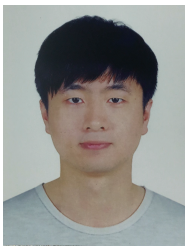

Anyue Wang (S'18-M'22) received his Bachelor and Master degrees in communication engineering from Beijing University of Posts and Telecommunications(BUPT), Beijing, China, in 2015 and 2018, respectively. He obtained his Ph.D. degree at the Interdisciplinary Center for Security, Reliability and Trust (SnT), University of Luxembourg, Luxembourg in 2022. From 2022 to 2023, he continued as a research associate at SnT, University of Luxembourg. His research interests include optimization and machine learning for resource management in wireless communication systems.

Lei Lei (S'12-M'17) received the B.Eng. and M.Eng. degrees from Northwestern Polytechnic University, Xi'an, China. He obtained the Ph.D. degree in 2016 at the Department of Science and Technology, Linköping University, Sweden. He was a research assistant at Institute for Infocomm Research (I2R), A*STAR, Singapore, in 2013. He was with the Interdisciplinary Centre for Security, Reliability and Trust (SnT), University of Luxembourg as a research associate and research scientist from 2016 to 2021. He is currently an Associate Professor with Xi'an Jiaotong University, School of Information and Communications Engineering. His current research interests include resource allocation and optimization in terrestrial-satellite networks, energy-efficient communications, and deep learning in wireless communications. He co-authored the IEEE ComSoc Best Readings in Satellite Mega Constellations and Non-Orthogonal Multiple Access. He received the IEEE Sweden Vehicular Technology-Communications-Information Theory (VT-COM-IT) joint chapter best student journal paper award in 2014. He was a co-recipient of the IEEE SigTelCom 2019 Best Paper Award.

Symeon Chatzinotas (S'06–M'09–SM'13) is currently Full Professor / Chief Scientist I and Co-Head of the SIGCOM Research Group at SnT, University of Luxembourg. In the past, he has been a Visiting Professor at the University of Parma, Italy and he was involved in numerous Research and Development projects for the National Center for Scientific Research Demokritos, the Center of Research and Technology Hellas and the Center of Communication Systems Research, University of Surrey. He received the M.Eng. degree in telecommunications from the Aristotle University of Thessaloniki, Thessaloniki, Greece, in 2003, and the M.Sc. and Ph.D. degrees in electronic engineering from the University of Surrey, Surrey, U.K., in 2006 and 2009, respectively. He was a co-recipient of the 2014 IEEE Distinguished Contributions to Satellite Communications Award, the CROWNCOM 2015 Best Paper Award and the 2018 EURASIP JWCN Best Paper Award. He has (co-)authored more than 400 technical papers in refereed international journals, conferences and scientific books. He is currently in the editorial board of the IEEE Open Journal of Vehicular Technology and the International Journal of Satellite Communications and Networking.

Björn Ottersten (S'87–M'89–SM'99–F'04) received the M.S. degree in electrical engineering and applied physics from Linköping University, Linköping, Sweden, in 1986, and the Ph.D. degree in electrical engineering from Stanford University, Stanford, CA, USA, in 1990. He has held research positions with the Department of Electrical Engineering, Linköping University, the Information Systems Laboratory, Stanford University, the Katholieke Universiteit Leuven, Leuven, Belgium, and the University of Luxembourg, Luxembourg. From 1996 to 1997, he was the Director of Research with ArrayComm, Inc., a start-up in San Jose, CA, USA, based on his patented technology. In 1991, he was appointed Professor of signal processing with the Royal Institute of Technology (KTH), Stockholm, Sweden. Dr. Ottersten has been Head of the Department for Signals, Sensors, and Systems, KTH, and Dean of the School of Electrical Engineering, KTH. He is currently the Director for the Interdisciplinary Centre for Security, Reliability and Trust, University of Luxembourg. He is a recipient of the IEEE Signal Processing Society Technical Achievement Award, the EURASIP Group Technical Achievement Award, and the European Research Council advanced research grant twice. He has co-authored journal papers that received the IEEE Signal Processing Society Best Paper Award in 1993, 2001, 2006, 2013, and 2019, and 8 IEEE conference papers best paper awards. He has been a board member of IEEE Signal Processing Society, the Swedish Research Council and currently serves of the boards of EURASIP and the Swedish Foundation for Strategic Research. Dr. Ottersten has served as Editor in Chief of EURASIP Signal Processing, and acted on the editorial boards of IEEE Transactions on Signal Processing, IEEE Signal Processing Magazine, IEEE Open Journal for Signal Processing, EURASIP Journal of Advances in Signal Processing and Foundations and Trends in Signal Processing. He is a fellow of EURASIP.